NIST Technical Note 1494

Measurement of yield stress for concentrated suspensions using a plate device

Chiara Ferraris
Min-Hong Zhang
Huaning Zhu
Vincent Picandet
Max A. Peltz
Paul Stutzman
Christina Arnaout
Daniel De Kee

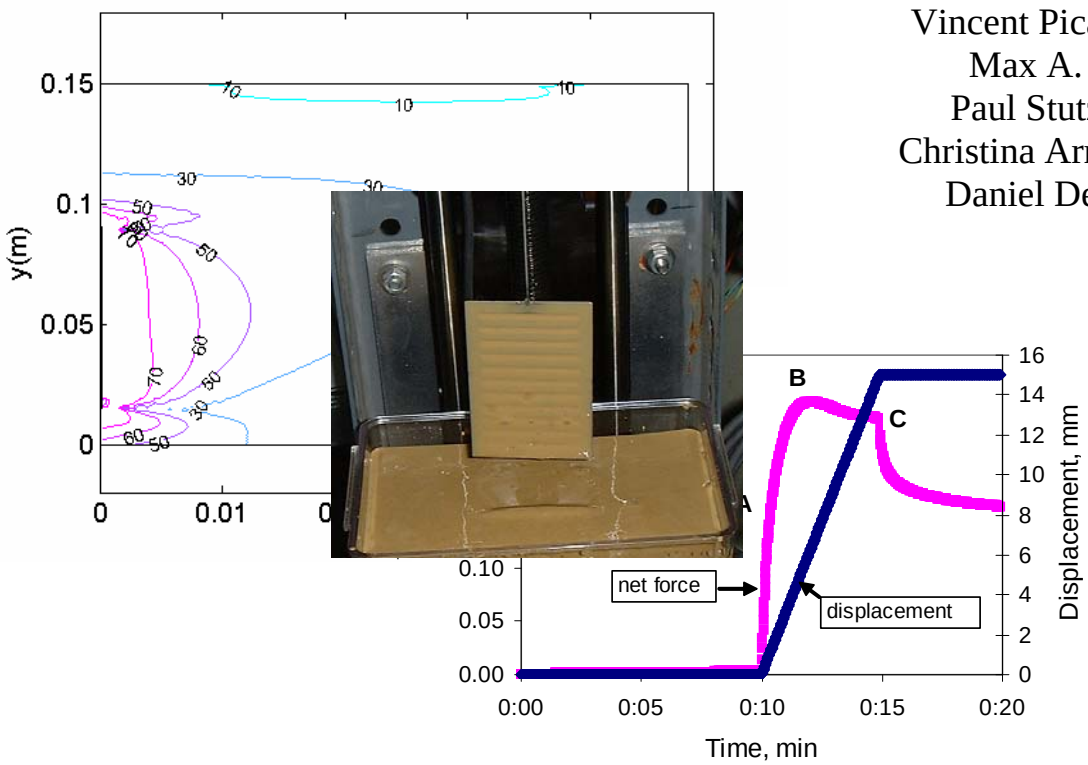

NIST National Institute of Standards and Technology • Technology Administration • U.S. Department of Commerce

NIST Technical Note 1494

Measurement of yield stress for concentrated suspensions using a plate device

Chiara Ferraris
Materials & Construction Research Division
Building & Fire Research Laboratory
Min-Hong Zhang
National University of Singapore, Singapore
Huaning Zhu
Materials & Construction Research Division
Building & Fire Research Laboratory
Vincent Picandet
Université de Bretagne Sud, Lorient, France
Max A. Peltz
Materials & Construction Research Division
Building & Fire Research Laboratory
Paul Stutzman
Materials & Construction Research Division
Building & Fire Research Laboratory
Christina Arnaout
University of Texas Austin, Austin TX
Daniel De Kee
Tulane University, New Orleans, LA

March 2008

U.S. Department of Commerce
Carlos M. Gutierrez, Secretary

National Institute of Standards and Technology
James M. Turner, Acting Director

Certain commercial entities, equipment, or materials may be identified in this document in order to describe an experimental procedure or concept adequately. Such identification is not intended to imply recommendation or endorsement by the National Institute of Standards and Technology, nor is it intended to imply that the entities, materials, or equipment are necessarily the best available for the purpose.

National Institute of Standards and Technology Special Publication XXXX
Natl. Inst. Stand. Technol. Spec. Publ. 1494, 42 pages (March 2008)
CODEN: NSPUE2

Abstract

Slump has often been correlated with the yield stress of concrete as defined by the Bingham model. The discussion is still open as to what the yield stress value actually is and how to measure the yield stress of a suspension in general and for a cementitious material in particular. A plate device is a recent development in the measurement of yield stress of suspensions that allows for testing at shear rates far below most rotational rheometers. This paper will present the plate device and the modifications made so that it can be used with suspensions such as bentonite or TiO_2 (Titanium dioxide) in aqueous solution, as well as portland cement in water. A careful analysis of the yield stress measurements will be discussed.

Keywords: Plate device, suspension rheology, yield stress, and smoothed particle hydrodynamics (SPH)

Acknowledgements

The authors would like to acknowledge support by the National University of Singapore for Dr. Zhang's sabbatical at National Institute of Standard and Technology (NIST), by the University of Brittany for Dr. Picandet's sabbatical and by Tulane University for Dr. Huaning Zhu's participation. Dr. Edward Garboczi and Nicos Martys review is appreciated as they allowed this paper to be improved.

Table of contents

1. Introduction 1
2. Background 2
3. Plate device and Test Method 5
   3.1. Equipment Design 5
   3.2. Principles of operation 7
   3.3. Calculation of Yield stress from the plate device tests 9
      3.3.1. Correcting the edge effect 9
      3.3.2. Slotted Plates 11
4. Experimental Study 12
   4.1. Materials used and mixtures 12
      4.1.1. Cement paste 12
      4.1.2. Bentonite 14
      4.1.3. Titanium Oxide 22
   4.2. Other rheometers used 22
5. Simulation of the plate device 23
6. Results and Discussion 30
   6.1. Determination of yield stress from the slotted plate device 30
      6.1.1. Interpretation of the measurements 30
      6.1.2. Edge effect correction 32
      6.1.3. Comparison of yield stress from the slotted and non-slotted plates 33
   6.2. Comparison of yield stress of the materials determined by different rheometers and methods 34
   6.3. Other observations from the tests using the plate device 35
      6.3.1. Force measured without plate movement 35
      6.3.2. Experimental issues with concentrated suspensions 37
7. Summary and Conclusions 39
8. References 40

List of tables

Table 1: Dimension of the plates. All plates are 1.2 mm thick and 50 mm wide 6
Table 2: Summary of the mixture used 12
Table 3: Composition of the cement based on two replicas measurements determined by X-ray powder diffraction. 13
Table 4: Parameters used in the numerical simulations 24
Table 5: Average shear stress along the plates of different length for Case I (bentonite suspension B1) 29
Table 6: Average shear stress along the plates of different length for Case II (bentonite suspension B3) 29
Table 7: Mean shear stress τ comparison (sand blasted plates). The uncertainty is estimated at 10 %. 32
Table 8: Mean shear stress τ comparison (smooth, non-sand blasted plates) The uncertainty is estimated at 10 %. 33
Table 9: Comparison of yield stresses determined by the slotted plate device and other rheometers. The uncertainty is estimated at 10 %. 35
Table 10: Yield stress and plastic viscosity of the suspensions determined by the co-axial rotational rheometer. The uncertainty is estimated at 10 % 36

List of Figures

Figure 1: Yield stress as function of plate speed related to shear rate for a TiO_2 suspension [3] 2
Figure 2: Schematic of a stress growth measurement. Point A is the end of the linear portion, i.e., elastic portion, and it is the static yield stress point; Point B is the peak point associated with the dynamic yield stress and it is taken as an approximation of the true yield stress because it is easier to determine 3
Figure 3: (a) Yield stress (σ_y) vs. slot ratio (β) for aqueous TiO_2 suspensions [3]. (b) Yield stress vs. slot ratio with two plate surface conditions for a 50 % mass fraction aqueous TiO_2 suspension [3]. 4
Figure 4: Experimental set-up (not to scale) 5
Figure 5: Slotted plate design (not to scale). L is the length of the plate and in our case (Table 1) could be 52 mm, 75 mm or 100 mm; Sst is the thickness of the outer frame (5 mm); St is the slot width and the Ss is the steel width. St and Ss vary depending on the number of slots. 7
Figure 6: Schematic strain ramp applied and typical force response obtained (bentonite suspension B1, tested with plate MPS) 9
Figure 7: Exerted forces on the plates 10
Figure 8: Typical graph of exerted forces on the plates of various lengths (bentonite suspension B1, tested with smooth plates). 10
Figure 9: Particle size distribution of the cement measured in isopropanol (IPA) by laser diffraction method. 13

Figure 10: Yield stress change with time for the cement paste for three different batches of the same mixture composition measured by stress growth method in a parallel plate rotational rheometer. 14
Figure 11: Bentonite particle size distribution in IPA by laser diffraction method. 15
Figure 12: Bentonite particle size distribution in water by laser diffraction method 15
Figure 13: Bentonite B1 oriented slide diffraction results for untreated, dry (black), ethylene glycol-water saturated (red), and heat-treated (550 °C, 1 h) in blue 17
Figure 14: Bentonite B3 X-ray powder diffraction patterns from oriented slides as dry (black), ethylene glycol – water saturated (red) and heat treated to 550 °C for 1 h (blue) 17
Figure 15: Bentonite B2 X-ray powder diffraction patterns from oriented slides as dry (black), ethylene glycol–water saturated (red) and heat treated (blue) 18
Figure 16: Ethylene glycol-water saturated oriented slides for bentonite B1 (black), clay B3 (red), and clay B2 (blue) shows the similarity when saturated for bentonite B2 and B3 and the broader diffraction peaks for bentonite B1 that reflect a lower ordering. 18
Figure 17: Bentonite B1 micrographs at lower (top) and higher (bottom) magnifications show the agglomerated nature of the grains (see micrographs for scale markers) ... 19
Figure 18: Bentonite B3 micrographs at lower (top) and higher (bottom) magnifications show the agglomerated nature of the grains (see micrographs for scale markers) ... 20
Figure 19: Bentonite B2 micrographs at lower (top) and higher (bottom) magnifications show the agglomerated nature of the grains (see micrographs for scale markers) ... 21
Figure 20: Comparison of shear stress versus shear rate for Case I (bentonite suspension B1). The experimental data were obtained using conventional rheometers (see section 4.2) 25
Figure 21: Comparison of shear stress versus shear rate for Case II (bentonite suspension B3). The experimental data were obtained using conventional rheometers (see section 4.2) 26
Figure 22: Contour plot of shear stress (Pa) for bentonite suspension B1 (case I). 26
Figure 23: Contour plot of shear rate (1/s) for bentonite suspension B1 (case I). 27
Figure 24: Contour plot of shear stress (Pa) for bentonite suspension B3 (case II). 27
Figure 25: Contour plot of shear rate (1/s) for bentonite suspension B3 (case II). 28
Figure 26: Stress distribution along plates of different lengths for case I (bentonite suspension B1). The top of the plate is at y =100 mm and the bottom of the plate is at y = 0. mm 28
Figure 27: Stress distribution along plates of different length for case II (bentonite suspension B3). The top of the plate is at y =100 and the bottom of the plate is at y = 0.mm 29
Figure 28: Comparison of typical curves of the force response with time determined from the plate device using the MPS plate (a) and those of the shear stress vs. shear rate determined from the co-axial cylinder rheometer (b). The data are from on measurements but the uncertainty is estimated to be 10 %. 31
Figure 29: Picture showing the bentonite suspension B1 on the smooth medium plate SL11 when the plate was pulled out of the suspension 34
Figure 30: Schematic model of well crystallized clay mineral [26] 36

1. Introduction

The workability of fresh concrete is an important property which affects consolidation, mechanical properties, and durability of concrete. From a rheological perspective, flow behavior of mortar and concrete is usually described by the Bingham model with two parameters - yield stress and plastic viscosity.

According to Hackley and Ferraris [1], the physical definition of the yield stress is the stress needed to initiate movement; therefore, it should be measured by slowly increasing the shear stress until movement occurs. This direct measurement is not easy to implement in most rotational rheometers because it implies that the shear stress is very well controlled. Most rheometers cannot control the stress with steps small enough to detect the yield stress.

Most commonly used rotational rheometers are coaxial or parallel plate types [2]. One difficulty in measuring the yield stress and plastic viscosity of suspensions using such equipment is the wall–sample interaction, which may result in slip effects. According to Zhu et al. [3, 4], wall depletion effects with multi-phase systems are associated with the displacement of the dispersed phase(s) away from solid boundaries, leaving a low-viscosity, particle-depleted layer near the wall. This phenomenon is due to surface, hydrodynamic, viscoelastic, chemical, and gravitational forces acting on the dispersed phase immediately adjacent to solid boundaries. The probability of wall slip increases when dealing with smooth walls, small flow dimensions, low flow rates, and suspensions of large or flocculated particles [5] . The low viscosity of the liquid near the wall leads to lower measured shear stress at a fixed shear rate, and therefore the viscosity and the yield stress are under-estimated [6]. A common way to avoid such complications is to roughen the surface of the walls in order to increase the sample-wall friction.

To overcome such complications, Zhu et al. [3, 4, 7] developed a plate device and method to measure the yield stress of suspensions using a controlled low shear rate. The novelty of the method is that the plate is a slotted plate, designed to create suspension/suspension shearing and not shearing between a “wall” and a suspension. This would hopefully eliminate the wall effect, and lead to a measurement of the true yield stress of a suspension. According to Zhu et al. [3], the method is particularly useful for measuring low-concentration suspensions with very low yield stresses. This method has been further developed by Picandet et al. [8] for concentrated suspensions such as cement pastes.

In this paper, the device built by Picandet et al. [8] at National Institute of Standard and Technology (NIST) from the design of Zhu et al. [3, 4, 9] is exploited to measure cement paste, bentonite and TiO_2 (titanium dioxide) suspensions. A systematic analysis of the experimental results and a computational simulation are presented with a critical discussion on the potential use of this device.

2. Background

The flow of a granular material such as cement paste (cement particles suspended in water) is difficult to measure due to the presence of particles. The overall behavior is non-Newtonian. The main characteristic of such a material is that it behaves as an elastic solid until it starts flowing. The shear stress at which the material starts flowing is called the yield stress. The yield stress is not easy to determine because the material needs to be sheared at very slow rate (zero shear rate limit) to capture it. Zhu et al. [3] have shown (Figure 1) that the yield stress depends on the static shear rate used until the shear rate is below a certain value. In the case of TiO_2 suspensions they found that the speed should be below 0.1 mm/min (1.7 x10^{-3} mm/s) for the new plate device. As very few instruments can shear at such low rate, it is not known whether this upper limit is material dependent. Obviously, the philosophical question arises as to whether knowing the true yield stress is necessary for engineering purposes as the material is seldom sheared at such low shear rates in a construction site.

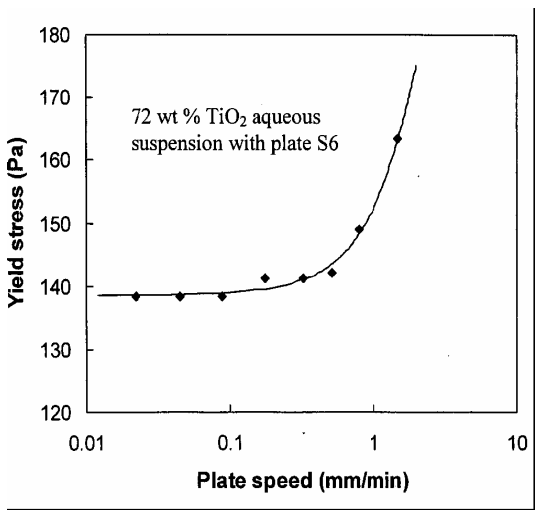

Figure 1: Yield stress as function of plate speed related to shear rate for a TiO_2 suspension [3]

Most commercially available rotational rheometers cannot achieve rotational speed low enough, therefore usually the yield stress is measured either by extrapolation to zero shear rate using the Bingham model [1, 10] or by stress growth (Figure 2) at a relative high speed in the order of 10 mm/s.

To measure the yield stress at very low shear rates, Zhu et al. [3, 4] developed a new device, called the plate device hereafter. This device is simple to build and adaptable to a wide range of granular materials. The device consists of a slotted plate submerged into a test material; the plate is slowly pulled out of the suspension while measuring the resistance of the material to this motion. The relationship of the stress versus time should be linear for an elastic material. Therefore, the yield stress is the point where the linearity is lost (point A in Figure 2). Zhu et al. [4] also showed that the shear stress at point A

does not change with shear rate applied, if the speed is low enough. On the other hand the stress at point B will depend on the shear rate applied.

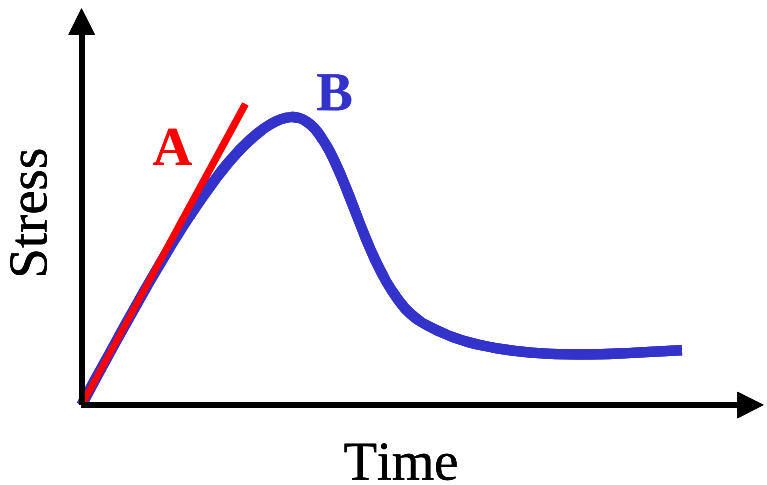

Figure 2: Schematic of a stress growth measurement. Point A is the end of the linear portion, i.e., elastic portion, and it is the static yield stress point; Point B is the peak point associated with the dynamic yield stress and it is taken as an approximation of the true yield stress because it is easier to determine.

The idea to pull or push an object into a suspension to determine the rheological parameters is not new. A review of these methods can be found in the ACI 238 [2] document. The idea is based on the falling ball rheometer and targets the measurement of viscosity by applying the Navier-Stokes law. In all cases, the speed is much higher than desired for a measurement of the yield stress. Another test that was very similar, in some ways is the Lombardi plate [11]. The test involved a plate with a rough surface attached to a balance. The plate was pulled out of the material and the mass of material attached to the plate was measured. There was no attempt to measure the force of moving the plate out of the material. Lombardi estimated that the amount of material sticking to the plate after removal from the suspension was related to the cohesion of the material and he showed that it was correlated with the yield stress measured using a Bingham model.

The key principle of the plate device [4] is that the speed can be easily controlled using a step motor (see section 3.1) and the plates can be modified to accommodate suspensions with different particle size distributions. To obtain the true yield stress the material should be sheared within the material and not between the material and an object, such as a plate. Therefore, ideally, a virtual plane of material should be moved inside the suspension and the material-material shearing stresses measured. Obviously, this is not possible in practice, so the virtual plate is approximated by a slotted plate. The slot area should be maximized while ensuring that there is no flow in the slots. The material in the slot behaves as a solid plate. Zhu et al. [3] through testing and simulation showed that the larger the slot area of the plate, the larger the measured yield stress (Figure 3 (a)) up to a value of slot ratio β ($\beta = S_{Bulk}/S_{Steel}$; where S_{Bulk} is the surface of the slot and S_{Steel} is the surface of the steel) of about 0.5. Therefore, a value of β higher than 0.5 (for TiO_2) measured the true yield stress of the material. At these values of β, the device was not

affected by slip. The yield stress in a suspension was always larger than the adhesive force between the suspension and the plate.

Zhu et al. [3] compared yield stresses determined using smooth stainless steel plates and sand-blasted Ti-Al alloy plates, and found that plate material properties as well as surface roughness also influence yield stress measurement. They suggested and confirmed (Figure 3 (b)) that the measured yield stresses of TiO_2 suspensions using two kinds of plates were very close to each other at high slot ratios while they could be significantly different at low slot ratios. This is attributed to the fact that true yield stress is independent of the plate condition as it should reflect the material-material shearing stresses as measured at high slot ratios.

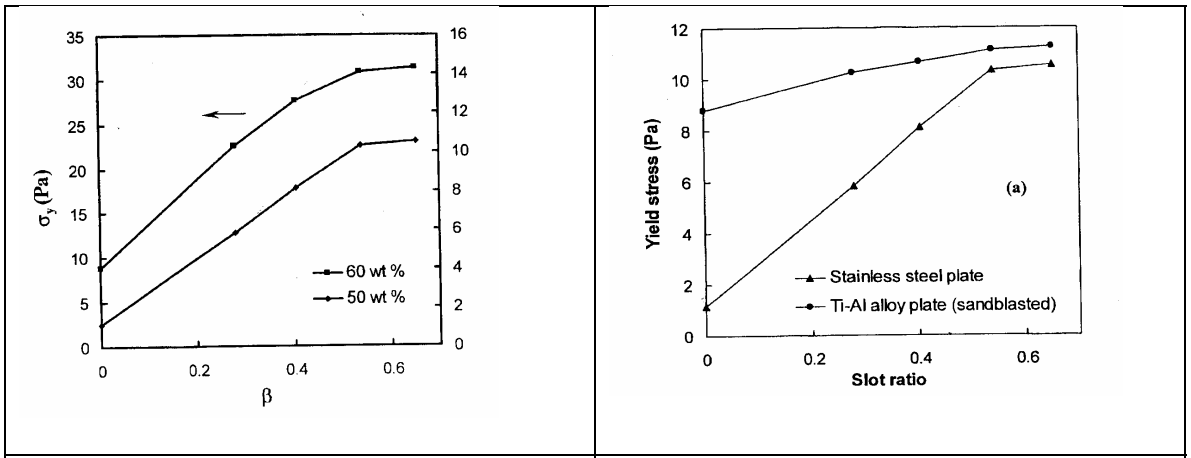

(a) (b)

Figure 3: (a) Yield stress (σ_y) vs. slot ratio (β) for aqueous TiO_2 suspensions [3]. (b) Yield stress vs. slot ratio with two plate surface conditions for a 50 % mass fraction aqueous TiO_2 suspension [3].

Other methods could be imagined to measure yield stress, such as oscillatory techniques, stress controlled/shear rate measurement or creep recovery [1] but the discussion of their advantages and disadvantages are beyond the scope of this paper. The goal here is to examine if the method developed by Zhu et al. could be applied to materials such as cement pastes or other pastes at similar volume concentrations. The determination of the true yield stress is essential in the description of the flow of suspensions such as cement paste.

3. Plate device and Test Method

3.1. Equipment Design

The instrument set-up from Zhu et al. [3, 4], was used for concentrated as well as very dilute suspensions. NIST built the device with some modifications to adapt it for more concentrated suspensions. The NIST device used consists of a container with the material to be tested placed on a platform that can move in the vertical direction, see Figure 4 [8]. The movement of the platform is controlled by a computer through a step-motor with a minimum speed of 0.05 mm/s. A balance is placed on a support on top of the container. The balance support cannot move and a hook below the balance suspends the plate.

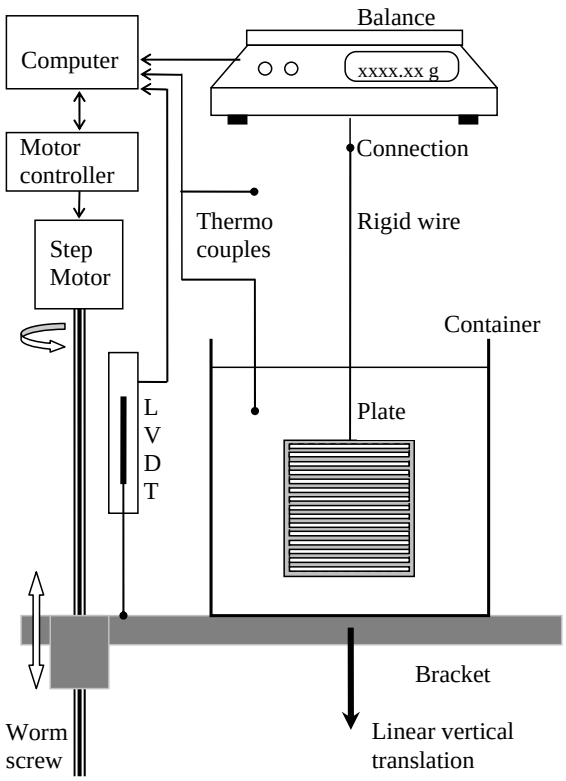

Figure 4: Experimental set-up (not to scale)

Various types of plates (slotted plates and solid plates of various lengths) were used to ensure that the measurement recorded the shear stress within the material. The slotted plates were used to create suspension/suspension shearing, whereas the solid plates were used to determine shear stress as between the plate and the suspension, as well as any correction factor that was needed due to the edge effect of the plates.

The plates were laser cut from a 1.2 mm thick and 50 mm wide stainless steel sheet. Some of the plates were sandblasted on both faces to roughen the surface and minimize slippage while others were used as is. The plates were of various lengths as shown in Table 1. For the slotted plates, 11 and 14 slots with a height of 3.05 mm and a width of 40 mm were laser cut and evenly distributed in the SL11 and SL14 plate, respectively.

It was determined [7, 8] that if the distance between the plate and the wall of the container was greater than 20 mm, the size and shape of the container had no influence on the results for the three kinds of suspensions investigated in this study.

Table 1: Dimension of the plates. All plates are 1.2 mm thick and 50 mm wide

	Name given to plates	
Length of plates/ slots number	**Sand blasted surface**	**Non sand blasted surface**
52 mm/ no slot	SPS	SP
75 mm / no slot	MPS	MP
100 mm / no slot	LPS	LP
75 mm /11 slots	SL11	
75 mm /14 slots		SL14

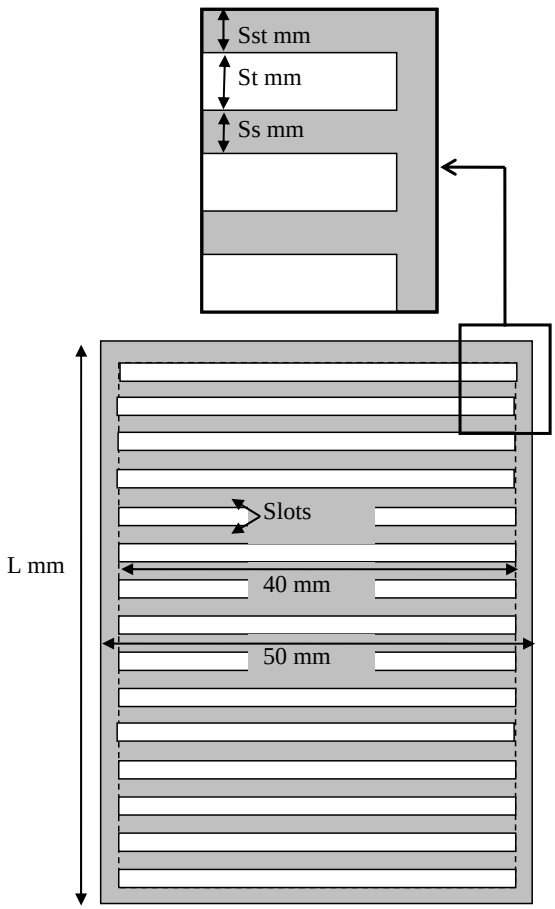

Figure 5: Slotted plate design (not to scale). L is the length of the plate and in our case (Table 1) could be 52 mm, 75 mm or 100 mm; Sst is the thickness of the outer frame (5 mm); St is the slot width and the Ss is the steel width. St and Ss vary depending on the number of slots.

3.2. Principles of operation

To initiate a test, the material is placed in the container and a plate is hooked to the bottom of the balance. The mass of the plate is recorded. The container is then lifted so that the plate is immersed at the desired depth. Vibration was applied to the suspension to ensure that the plate was as vertical as possible. The plate was at rest in the suspension for the first 10 min to ensure equilibrium. The platform with the container was then moved downwards at a speed of 0.05 mm/s for 5 min, thus the container moved 15 mm. This was followed by a rest of 5 min. Total time for each test was 20 min. The temperature of the suspension was monitored by a thermocouple during the test and recorded.

Specialized software[1,2] was developed to interface with the measurements and control the step motor moving of the platform supporting the container. The software was able to record the speed, and displacement of the platform, the temperature of the suspension, and the output of the balance.

When the plate is immersed in the material and the container is slowly moved downwards, the material in the container exerts a force on the plate. The plate in turn exerts a force on the balance, and the resulting force and corresponding displacement are recorded by a computer in real time. The movement of the platform is measured by a linear variable differential transformer **(**LVDT) and controlled by a computer through a step motor.

The force and corresponding displacement are recorded by a computer, and plotted against time as shown in Figure 6. At first, the measured force increases almost linearly with time, confirming the elastic nature of the material before yielding. At Point *A* (Figure 2), the slope of the curve begins to decrease, and the Force-Time curve deviates from linearity. Just before the stress reaches its maximum, the slope of the curve decreases significantly, and the non-linear behavior between Points *A* and *B* is likely associated with structural rearrangement [3]. At the maximum stress, the structure is destroyed and the suspension flows. The region between Points *B* and *C* reflects the thixotropic nature of the suspension. If the strain is stopped at Point *C*, a stress relaxation will be recorded. The remaining stress recorded at the end of the test is associated with a residual stress, which cannot be used to compute a reliable value of yield stress because of the thixotropic nature of these kinds of suspensions.

Zhu et al. [3] have shown that the maximum stress depends on the strain rate, but that at a sufficiently low speed, around 0.01 mm/s for TiO_2 suspension, the yield stress ceases to be a function of platform speed (Figure 1). However, the rheological properties of cement paste samples change with time to the hydration kinetics of cement paste. To consider constant properties during testing, the platform speed has been selected to be 0.05 mm/s. A lower speed would not allow one to clearly observe a maximum stress as shown in Figure 6.

From the force recorded when the plate moves in a suspension, shear stress τ can be calculated using Eq. (1), and shear stress-time curves can be plotted.

$$\tau = F_R / S = (F - F_i) / 2WL \qquad \textbf{[1]}$$

where F_R : measured net force,
S : surface area of the plate,

---

[1] LabView was used as the tool for the software[2].

[2] Commercial equipment, instruments, and materials mentioned in this report are identified to foster understanding. Such identification does not imply recommendation or endorsement by the National Institute of Standards and Technology (NIST), nor does it imply that the materials or equipment identified are necessarily the best available for the purpose.

F : measured force using balance,
F_i: initial force (= gravitational force due to plate and wire mass - the buoyant force in suspension),
L : length of the plate, and
W : width of the plate.

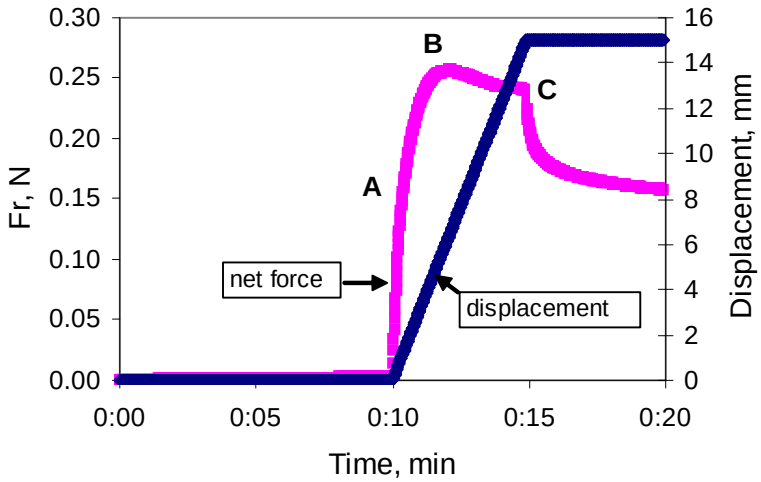

Figure 6: Schematic strain ramp applied and typical force response obtained (bentonite suspension B1, tested with plate MPS)

3.3. Calculation of Yield stress from the plate device tests

3.3.1. Correcting the edge effect

Smooth plane plates of varying length were used to determine the drag forces exerted on the plate edges and to evaluate τ_S, the stress from the steel surface. When the plate moves upward, its upper edge displaces the suspension and there are drag forces exerted on the lower edge F_{el} and upper edge F_{eu} of the plate, (see Figure 7).

$$F_R = F_{eu} + F_{el} + 2WL\tau_S \qquad [2]$$

where F_R : measured net force at the yield point,
F_{el}: Force exerted at the lower edge
F_{eu}: Force exerted at the upper edge
L : length of the plate,
W: plate width, and
τ_S : yield stress associated with the surface 2WL.

W, τ_S and the sum of the drag forces $F_D = F_{eu} + F_{el}$ is constant for a given mix. The series of stainless steel plates with different lengths but same edge dimension, geometry and

surface conditions were used to correct for the edge effect by plotting F_R versus L which generated a straight line with intercept F_D and with a slope related to τ_S (Figure 7, Figure 8)

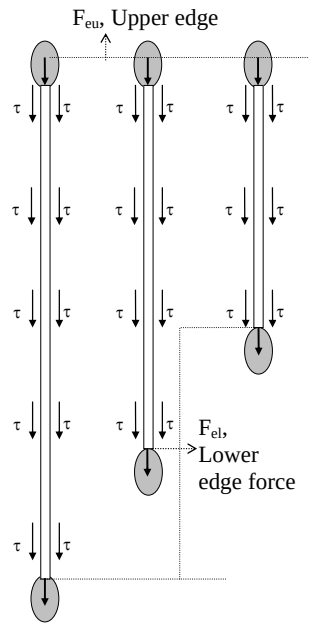

Figure 7: Exerted forces on the plates

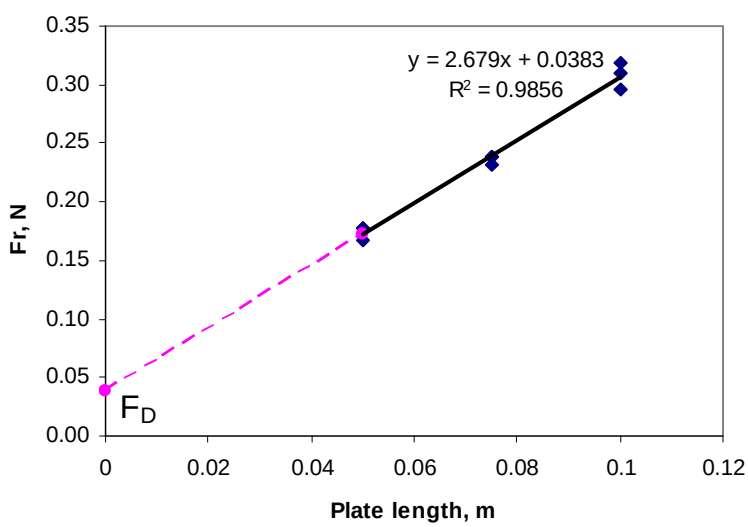

Figure 8: Typical graph of exerted forces on the plates of various lengths (bentonite suspension B1, tested with smooth plates).

3.3.2. Slotted Plates

To analyse the slippage effect, a series of parallel and horizontal slots were opened on a medium sized plate. It was assumed that when the slotted plate moves in the material, the suspension in a slot remains static relative to the plate. Zhu et al. [7] have shown that if the ratio of the height of a slot over the thickness of the plate is smaller than 3, the suspension filling the slots can be considered static, with no secondary flow and with shearing occurring only at the edge of the slots.

Using the slotted plate, the true suspension yield stress τ_B is measured at the interface of the suspension inside the slots and the adjacent bulk. The mean stress exerted on the plate is the combination of the yield stress τ_B over an area S_{Bulk} and τ_S over an area S_{Steel}. τ_S is assumed to be lower than τ_B due to slip. The mean shear stress τ exerted on the plate is a function of the area ratio $\beta = S_{Bulk}/S_{Steel}$, τ_S, and the parameter to measure, τ_B as shown in equation 3:

$$\tau = \left[\beta\tau_B - (1-\beta)\tau_S\right] \qquad \textbf{[3]}$$

And the force F_R exerted on the plate is (Eq. 4):

$$F_R = 2WL\left[\beta\tau_B - (1-\beta)\tau_S\right] + F_D \qquad \textbf{[4]}$$

The drag force F_D depends on the sample as well as on the operating conditions such as plate speed and test temperature, but it is not a function of the slot ratio β since the suspension in the slots moves with the plate. The ideal situation would refer to a virtual sample plate moving through the sample.

Two slotted plates (Table 1) were used: 1) a sand blasted surface with a ratio $\beta = 0.358$ (SL11) and 2) a smooth surface with a $\beta = 0.455$ (SL14). The measurements with the two plates allow for the extrapolation of the contribution of the slip effect and to deduce the yield stress τ_B of the suspension [7]. The slotted plates were designed such that the ratio of the height of the slots over the thickness of the plate is smaller than 3, and the slot height was at least 100 times larger than the particle size in the suspensions [3]. These conditions were met to strengthen the assumption that the suspension in the slots is static with no secondary flow and the shear occurs only at the edge of the slots (material in the slot shearing against the material in the bulk). The method also assumes that the structure of the suspension in the slots is identical to that of the bulk suspension, and that the stresses τ_S and τ_B are independent.

4. Experimental Study

4.1. Materials used and mixtures

An ASTM Type I normal portland cement, three bentonites, and a commercial TiO_2 pigment[3] were used in this research.

Table 2 summarizes the mixtures. The details on how the mixtures were prepared and on the composition of the various materials are given below.

Table 2: Summary of the mixture used

Solid particles	Water/Solid ratio [by mass]	Additives and dosage [% of solids by mass]	Volume concentration of solids [%]
Cement	0.33	Retarder (0.19 %)	48
Bentonite B1	9.0[#]	--	4.0
Bentonite B2	9.3	--	3.1
Bentonite B3	9.3	--	3.1
TiO_2	1.0	--	20

[#] The mass concentration of bentonite B1 suspension was determined by averaging three tests as the moisture content of B1 was not measured prior to preparing the suspension.

4.1.1. Cement paste

The cement used had a composition as shown in Table 3. The particle size distribution (PSD) is shown in Figure 9. The surface area calculated from the PSD was 541 m^2/kg.

The cement paste suspension had a water/cement (w/c) ratio of 0.33 by mass. This 48 % concentration by volume in water can be considered to be a high concentration suspension. A retarder admixture was added to allow for a longer time to conduct the measurements.

Cement paste was mixed with a Hobart[2] mixer for about 4 min initially, and then mixed intermittently every 5 min until about 34 min from the time water was in contact with the cement. A retarding admixture was added in the mixing water to delay the onset of cement hydration, so that workability of the cement paste remained almost constant during a period of about 3.5 h. After mixing, the paste was transferred to a plastic container with a diameter of approximately 115 mm.

Yield stress was also determined via a parallel plate rheometer [10] up to about 7 h, and the results are plotted in Figure 10. The results indicate that the yield stress did not change

[3] TiO2 was from Tronox CR-826[2]

significantly with time during the first 4 h. The tests by the plate device, therefore, were conducted between about 45 min to 3 h after water and cement were in contact. The jar with the cement paste was shaken manually before each subsequent test.

Table 3: Composition of the cement based on two replicas measurements determined by X-ray powder diffraction.

Components	Mass Fraction [%]	Standard Deviation [%]
alite	58.1	11
belite	19.3	2
aluminate	2.7	4
ferrite	12.1	4
periclase	3.4	2
arcanite	0.4	4
gypsum	1.1	8
bassanite	2.3	6
anhydrite	0.5	1
quartz	0.1	0

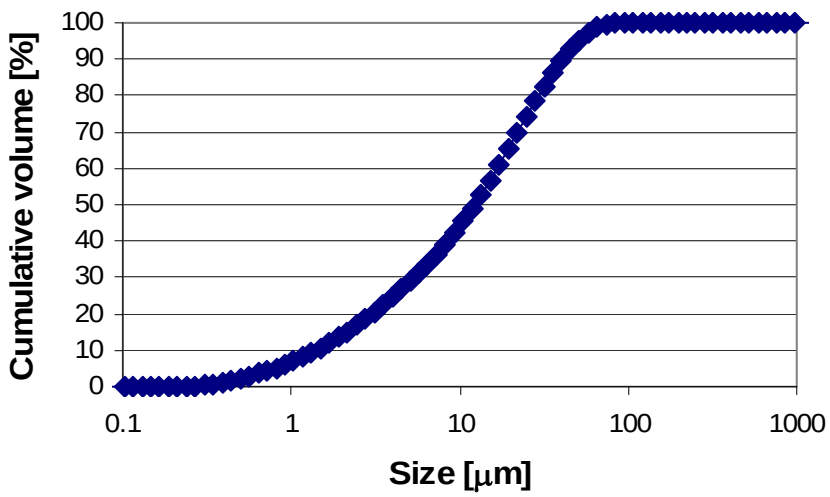

Figure 9: Particle size distribution of the cement measured in isopropanol (IPA) by laser diffraction method.

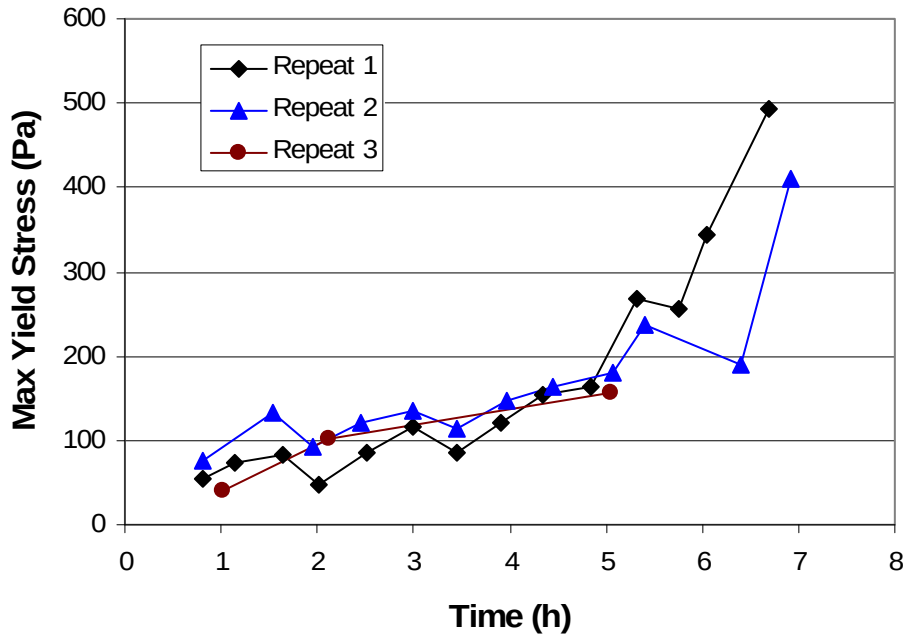

Figure 10: Yield stress change with time for the cement paste for three different batches of the same mixture composition measured by stress growth method in a parallel plate rotational rheometer.

4.1.2. Bentonite

Three bentonites of different origins were used: B1 (France), B2 and B3 (USA). Bentonite was selected because it is similar to cement with regards to particle size distribution but it does not react with water and therefore its properties do not evolve with time as in cement paste. Nevertheless, the particles absorb water slowly, which could result in changes in the measured properties over a period of time, but usually measured in months rather than in hours like in cement paste. All three materials were mostly pure commercial bentonites with no additives added with the particle size distribution of each bentonite are shown in Figure 11 as measured in isopropanol (IPA) and in Figure 12 as measured in water. For the measurements in water, bentonite slurry that was over a year old was sampled and placed in the laser diffraction device for measurements. It can be seen that although the three bentonite particle size distribution seem identical when measured in IPA they are quite different when measured in water. It seems that B1 can disperse better and the particle size is smaller than for B2 and B3. This could partially explain the very different rheological behavior observed for B1 compared to B2 and B3.

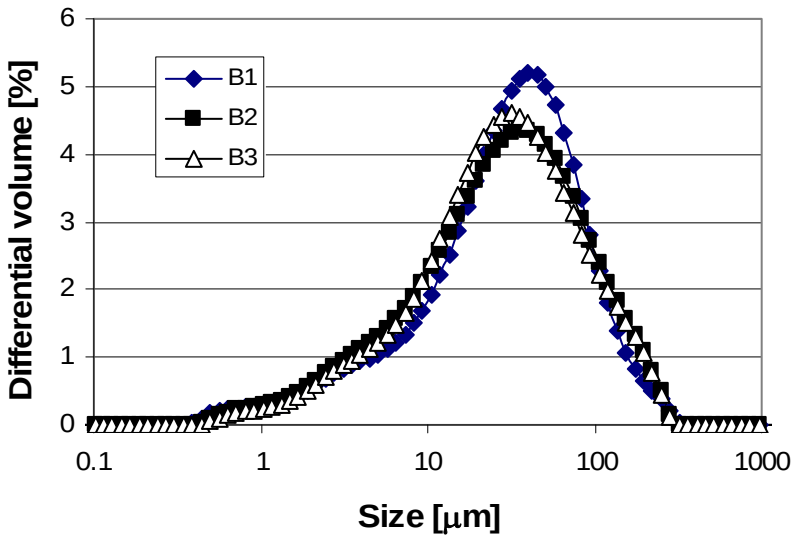

Figure 11: Bentonite particle size distribution in IPA by laser diffraction method.

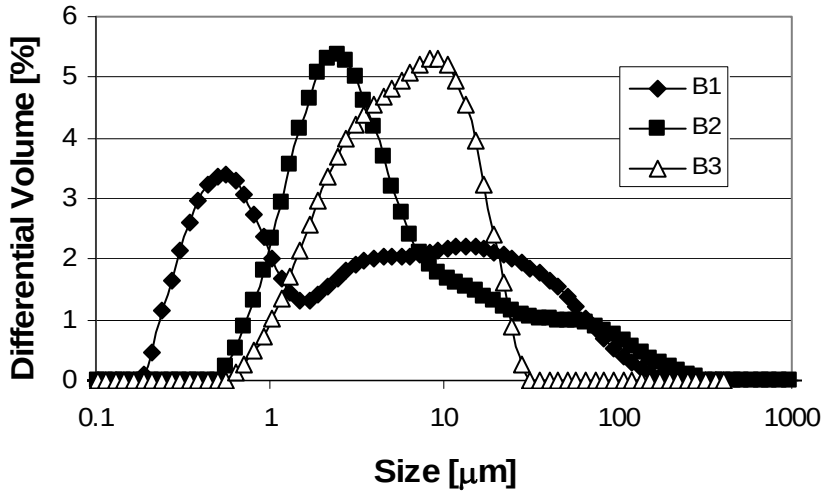

Figure 12: Bentonite particle size distribution in water by laser diffraction method

The density was tested after the material was dried in an oven at 105 °C for 4 h and then kept in a dessicator for 2 days. A Le Chatelier flask with IPA was used to measure the particles density. The values obtained were:

- B1: 2660 kg/m^3 ± 20 kg/m^3
- B2: 3425 kg/m^3 ± 20 kg/m^3
- B3: 3415 kg/m^3 ± 20 kg/m^3

The moisture in the bentonite was measured by drying the material at 105 °C overnight and was found to be 9.3 % for B2 and 7.5 % for B3 by mass. The uncertainty is estimated at 0.1 %. B1 moisture was not measured.

Bentonite suspensions B2 and B3 were prepared in the 2 L-plastic containers and the containers were capped and rotated on a 3D mixer[4] intermittently with a roller for at least two months before the suspensions were used for testing. Bentonite B1 was tested after about one year. The suspension was mixed on the 3D mixer for 0.5 h before the tests each day, and manually shaken between each test during the day. Bentonite suspensions of B1 and B2/B3 had volume concentrations of 4.0 % and 3.1 %, respectively (Table 2).

Bentonite composition

The phase composition was measured by X-ray diffraction (XRD) using oriented clay mounts. A few grams of bentonite were suspended in distilled water with some ultrasonic agitation to facilitate de-agglomeration. The suspension was pipetted to a glass slide and allowed to dry as the bentonite particles settled, enhancing the (00L) reflections for identification. This involves diffraction scans of three treatments; one in a dry condition, one after saturation with an ethylene glycol-water 1:1 mixture to expand expandable layers, and one heated to 550 °C to collapse the expandable layers. The expansion and collapse is seen by the shifting of the basal plane diffraction peaks and is diagnostic in phase identification. Diffraction patterns for each clay sample are provided in Figure 13 to Figure 15 with the room-condition scan in black, the glycol-saturated scan in red, and the heat-treated scan in blue. An additional figure of the glycol-saturated patterns for each specimen illustrates the similarities and differences best (Figure 16).

Montmorrillonite group clays are the predominant clay mineral in bentonites [12]. All three glycol-saturated bentonites show the similarity between B2 and B3 and the broader peaks of B1 that indicate a poorer ordering (sometimes called crystallinity) and wider range of d-spacings upon saturation. The patterns each indicate a montmorrillonite group clay with the (001) peak for each specimen at 1.3 nm along with the (002) peak around 0.87 nm and the (003) peak at 0.34 nm. The (001) peak shifts to about 1.7 nm on glycol saturation and to 0.97 nm on heat treatment. There also are indications of a second clay type in sample B1, with a 2.4 nm peak in the dry specimen that does not appear to shift upon saturation, possibly an ordered mixed layer clay that is not expandable. Sample B1 appears to contain minor amounts of quartz while samples B3 and B2 contain some potassium feldspars. Micrographs of each of the clays indicate that the powders are comprised of agglomerates of clay particles [Figure 17 to Figure 19] with no clearly discernable platy habit of the clay particles due to their fine size.

[4] A Turbula was used for this mixing[2].

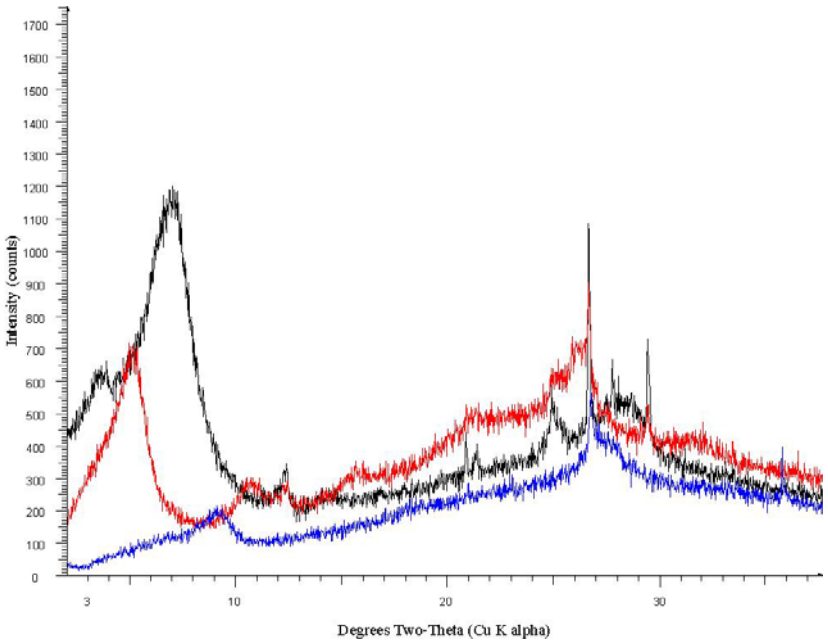

Figure 13: Bentonite B1 oriented slide diffraction results for untreated, dry (black), ethylene glycol-water saturated (red), and heat-treated (550 °C, 1 h) in blue

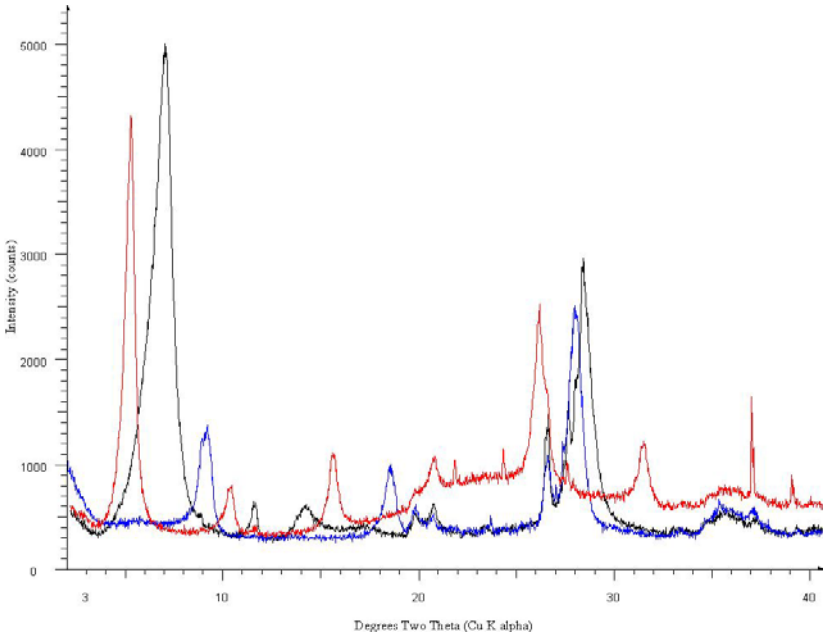

Figure 14: Bentonite B3 X-ray powder diffraction patterns from oriented slides as dry (black), ethylene glycol – water saturated (red) and heat treated to 550 °C for 1 h (blue)

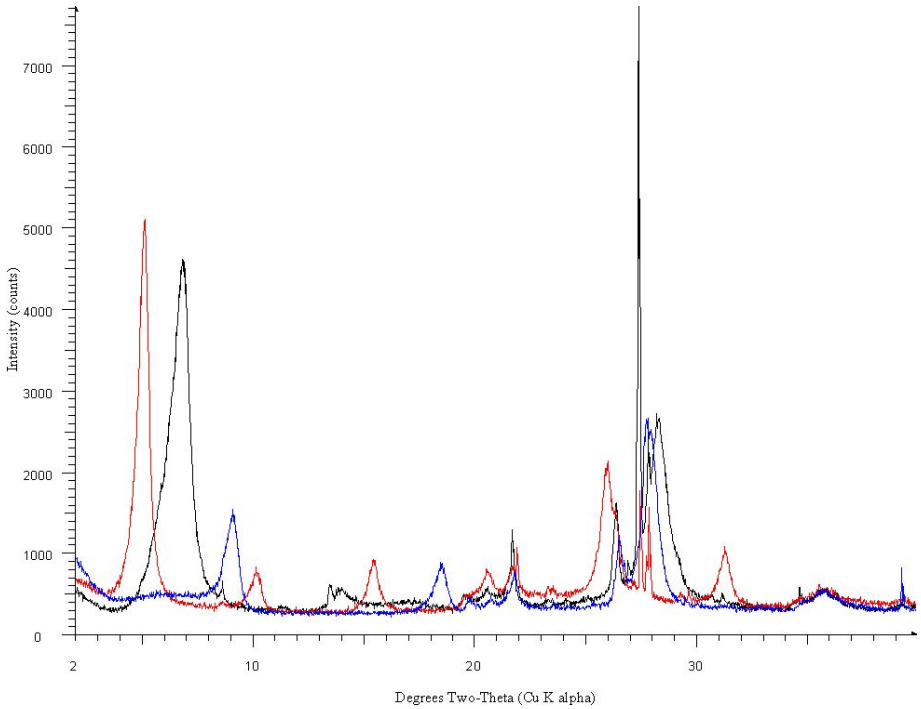

Figure 15: Bentonite B2 X-ray powder diffraction patterns from oriented slides as dry (black), ethylene glycol–water saturated (red) and heat treated (blue)

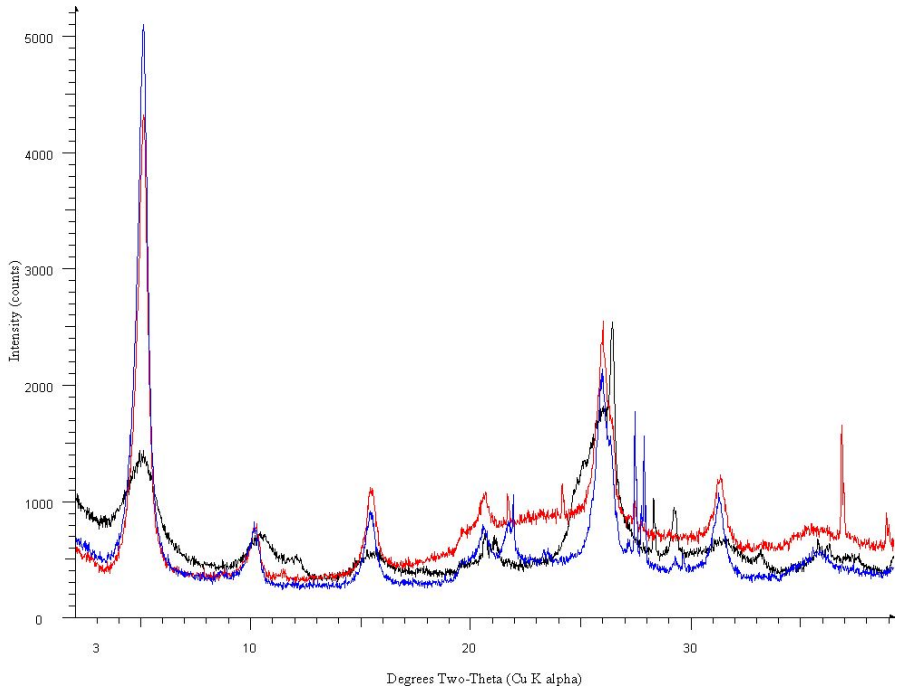

Figure 16: Ethylene glycol-water saturated oriented slides for bentonite B1 (black), clay B3 (red), and clay B2 (blue) shows the similarity when saturated for bentonite B2 and B3 and the broader diffraction peaks for bentonite B1 that reflect a lower ordering.

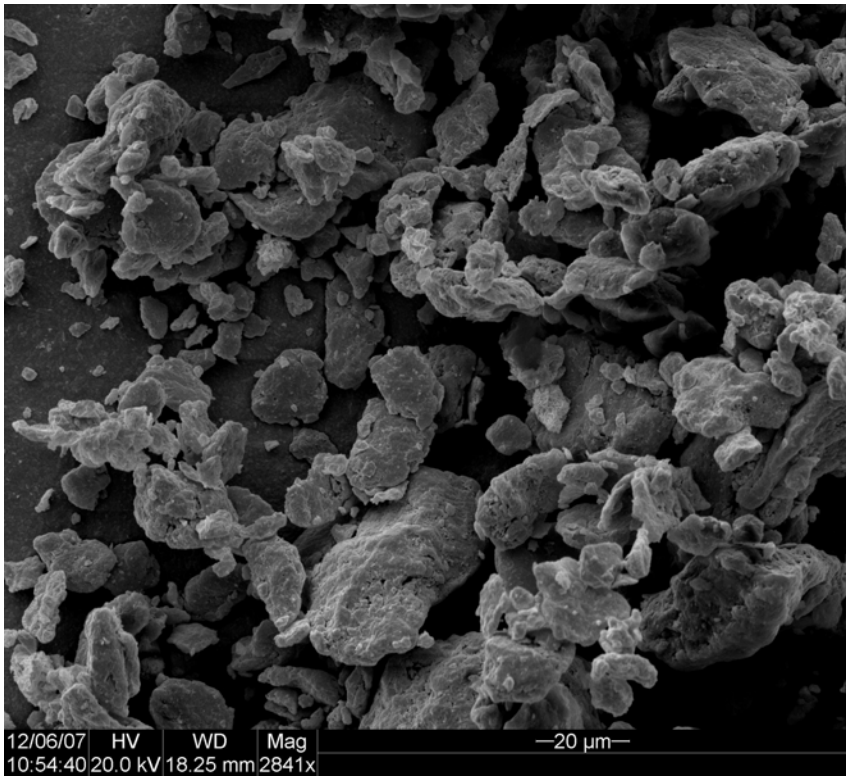

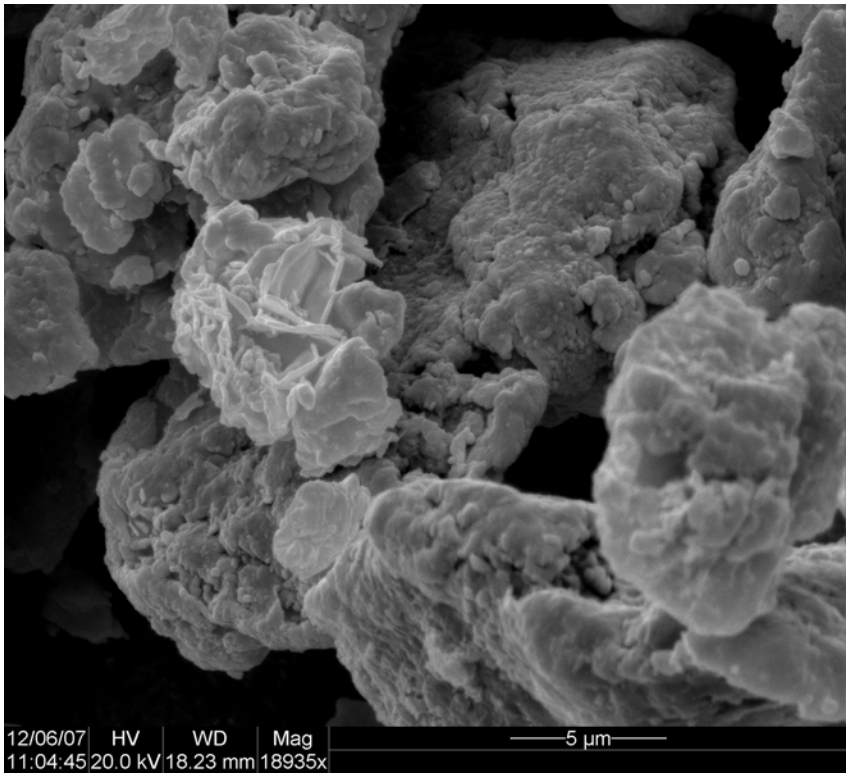

Figure 17: Bentonite B1 micrographs at lower (top) and higher (bottom) magnifications show the agglomerated nature of the grains (see micrographs for scale markers)

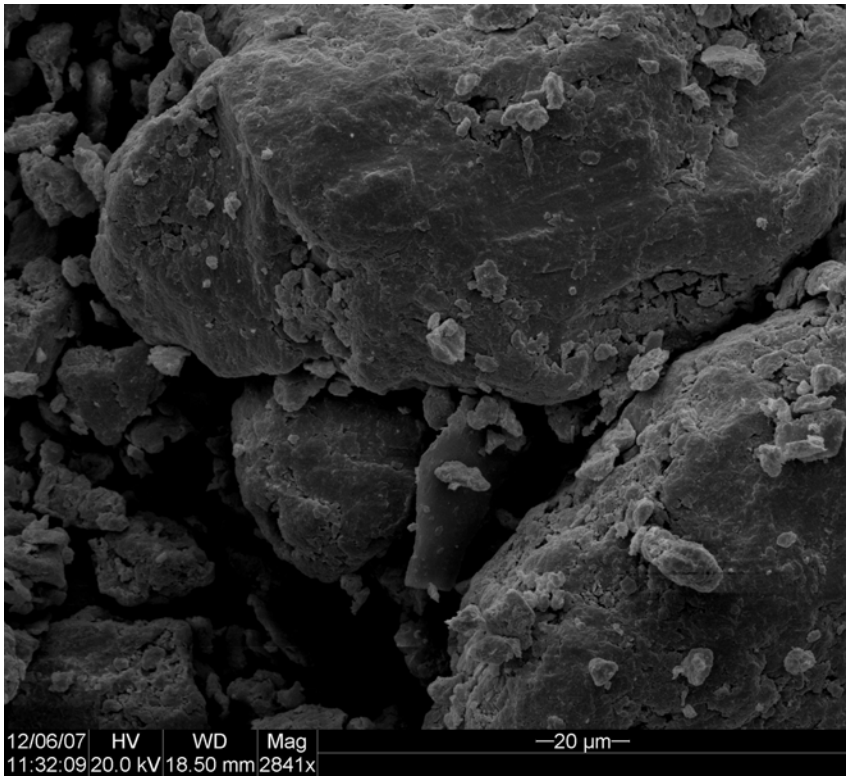

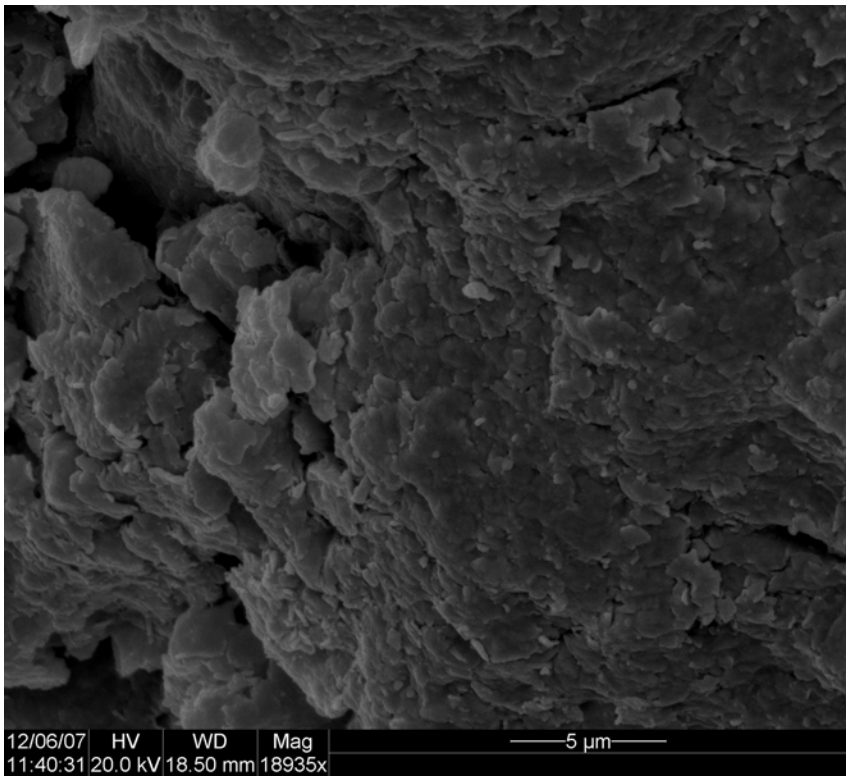

Figure 18: Bentonite B3 micrographs at lower (top) and higher (bottom) magnifications show the agglomerated nature of the grains (see micrographs for scale markers)

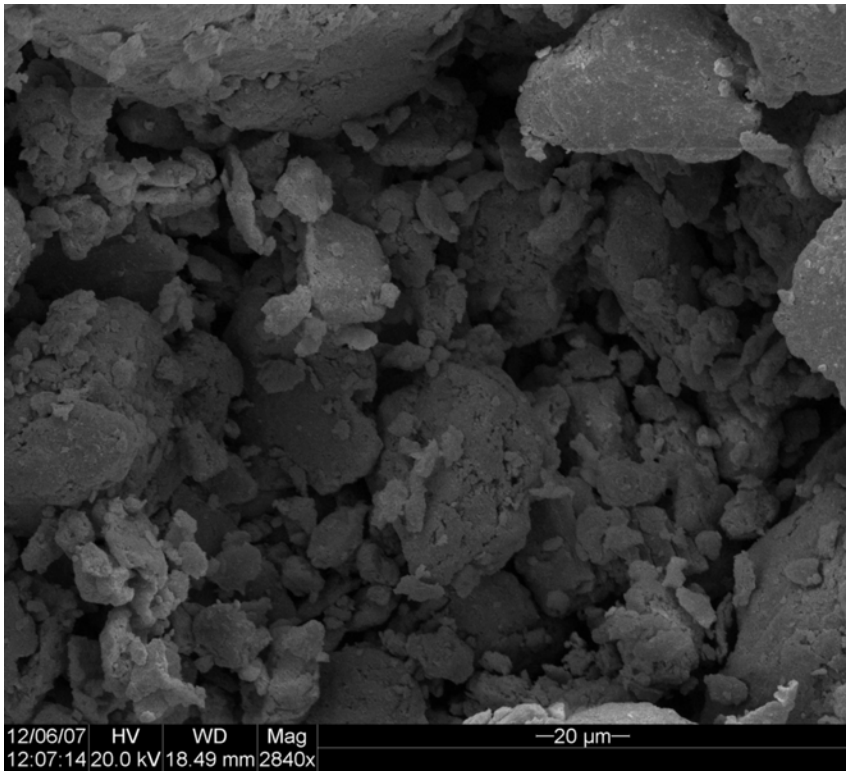

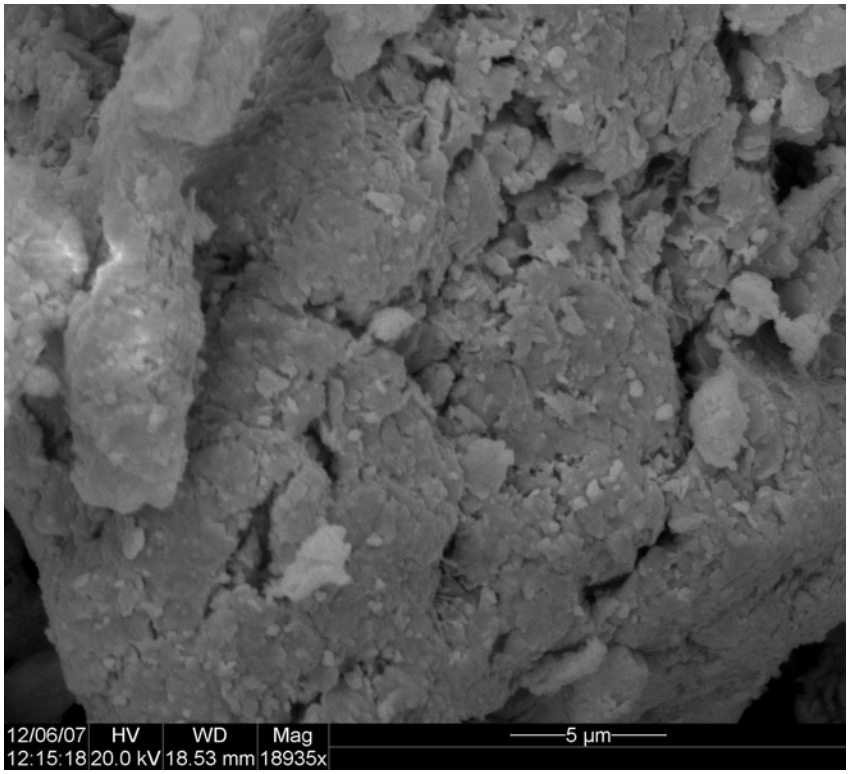

Figure 19: Bentonite B2 micrographs at lower (top) and higher (bottom) magnifications show the agglomerated nature of the grains (see micrographs for scale markers)

4.1.3. Titanium Oxide

The suspension was prepared from a commercial titanium oxide (TiO_2) pigment according to Ref. [13]. The solid particles had a specific gravity of 4.0 and contained 93 % TiO_2 mass fraction with an average diameter of 0.2 μm. Aqueous 0.01 mol/L KCl solution was used as the dispersing medium to prepare a suspension with a mass concentration of 50 % solids (volume concentration of solids = 20 %). The suspension was prepared in a 2L-plastic container and the containers were capped and rotated on a $3D^4$ mixer initially for 1 h. Afterwards, the suspension was mixed intermittently by hand for at least 30 s before each tests. The pH of the suspension was adjusted to 7.0 by adding HCl and KOH. All the tests were conducted within 48 h after the TiO_2 suspensions were prepared.

4.2. Other rheometers used

A rheometer that consists of two 35 mm, stainless steel serrated, circular parallel plates was used to determine the yield stress based on a stress growth procedure [10]. The top plate rotates at a controlled shear rate and the torque generated from the resistance of the material tested was measured on the top plate. The bentonite suspensions and cement paste were measured using this system. Due to the difficulty in cleaning the plates, disposable plates of 60 mm in diameter were used to test the TiO_2 suspensions. The temperature was controlled at 23 ^oC $\pm$ 2 ^oC. The details of the rheometer are described in References [10, 14].

The same rheometer but with a coaxial cylinder configuration was used to determine the yield stress and plastic viscosity of the suspensions based on the Bingham model. The shear rate controlled coaxial cylinder was used. The cylindrical container had an outer diameter of 43 mm. The rotor cylinder had a length (16 mm) and a diameter (22 mm). The rotor had smooth walls as it is customary in a coaxial cylinder rheometer. The torque resulting from the material resistance was measured at the central rotating tool. The shear rate was first changed gradually from 0.5 s^{-1} to 50 s^{-1}, and then decreased gradually to 0.5 s^{-1}.

5. Simulation of the plate device

The smoothed particle hydrodynamics (SPH) approach [15, 16] was used for the numerical simulation. As a Lagrangian based approach, the SPH method removes the difficulties associated with convective terms and allows one to tackle flow problems involving large deformation and free surfaces in a relatively natural way. The tensorial continuum and momentum equations have the form:

$$\frac{d\rho}{dt} = -\rho \nabla \cdot \boldsymbol{v} \qquad [5]$$

$$\frac{d\boldsymbol{v}}{dt} = \nabla \cdot \boldsymbol{P} + \boldsymbol{b} \qquad [6]$$

where $\boldsymbol{P} = -p\boldsymbol{I} + \boldsymbol{\tau}$, p is the hydrostatic pressure at equilibrium and $\boldsymbol{\tau}$ is the extra stress tensor. For an idealized Herschel-Bulkley fluid, the constitutive equation can be written as:

$$\boldsymbol{\tau} = \left(\eta \dot{\gamma}^{n-1} + \frac{\tau_0}{\dot{\gamma}} \right) \dot{\boldsymbol{\gamma}} \text{ for } \tau > \tau_0, \qquad [7]$$

$$\dot{\boldsymbol{\gamma}} = 0 \quad \textbf{for } \tau < \tau_0,$$

where $\dot{\boldsymbol{\gamma}}$ is the strain rate tensor, η is the plastic viscosity, τ_0 is the yield stress, n is the power law index and $\dot{\gamma} = \frac{1}{2}\sqrt{\dot{\boldsymbol{\gamma}} : \dot{\boldsymbol{\gamma}}}$ and $\tau = \frac{1}{2}\sqrt{\boldsymbol{\tau} : \boldsymbol{\tau}}$. Note that when the parameter n is equal to 1, the Bingham model is recovered. It is difficult to apply the Herschel-Bulkley / Bingham models directly in numerical simulations, especially in complex geometries. The difficulty is mainly due to the fact that the shape and location of the yield surface are *priori* unknown when calculating the velocity field. In the present study, the regularized Herschel-Bulkley model [17, 18, 19, 20] was adopted to overcome the numerical difficulties. The regularized Herschel-Bulkley model can be written as:

$$\boldsymbol{\tau} = \left(\eta \dot{\gamma}^{n-1} + \tau_0 \frac{\left[1 - e^{-m\dot{\gamma}}\right]}{\dot{\gamma}} \right) \dot{\boldsymbol{\gamma}} \qquad [8]$$

In the present study, the parameters τ_0 , η , n and m were chosen based on the experimental data of bentonite suspensions B1 and B3 using a coaxial rheometer. Figure 20 and Figure 21 compare the results from Eq. 4 with the experimental data. The parameters used in Eq. 8 are listed in Table 4. Note that in case II, the power law index is equal to 1, i.e. a Bingham model was used to characterize the bentonite materials.

Table 4: Parameters used in the numerical simulations

	τ_0 (Pa)	η (Pa·s)	n	M
Case I (B1)	27.0	8.0	0.47	500
Case II (B3)	76.2	0.5	1	1000

The numerical simulation was performed for the flow of suspensions in a two-dimensional domain. The upper surface was considered to be free and the symmetry condition with respect to the y-axis is applied on the left surface, that is to say only half of the geometry is considered (See Figures 22-25). The simulation domain was 48 mm in width and 150 mm in height, with a total number of 20000 SPH particles interacting with each other via the SPH equations. A 0.6 mm thick and 150 mm long plate was placed vertically on the left surface with a distance of 15 mm between the bottom end of the plate and the bottom surface of the container. Non-slip boundary conditions were imposed on the right and bottom walls. During the experiment, the plate was moved upwards with a constant velocity of 0.05 mm/s.

Figure 24 and Figure 25 show the shear stress and the shear strain distribution for the bentonite suspension B1, respectively, which were obtained by using the regularized Herschel-Bulkley model. Specifically, Figure 22 shows the contour plot of the shear stress distribution for the bentonite suspension B1. The shear stress is uniformly distributed along the surface of the plate except for the regions close to the upper and bottom ends. The stress concentration in those locations is an indication of disturbance of flow by the upper and bottom edges of the plate. Figure 23 shows that the shear rate is not linearly distributed along the x-direction and it is confined in a region close to the surface of the plate. It is also noted that in case I, the average shear stress along the plate surface is 19.9 Pa, which is below the yield stress obtained by interpolation (Table 4). Note that in the numerical simulation a Papanastasiou type constitutive model (Eq. 8) is adopted, therefore it is possible that the computed stress is less than the yield stress τ_0 when the shear rate is extremely low Figure 24 and Figure 25 show the shear stress and the shear strain distribution for bentonite suspension B3, which is computed by using the regularized Bingham model. Similar to the previous case, the stress and the shear rate are uniformly distributed along a major part of the plate surface. As the horizontal distance to the plate becomes larger, the stress and shear rate drop substantially. The average shear stress along the plate surface is 76.6 Pa in case II, which is greater than the yield stress. This indicates that there is a thin layer of material along the plate surface whose stress is above the yield stress and the material within this band flows as a fluid.

The numerical simulations for these two suspensions using plates with different lengths of 50 mm, 75 mm and 100 mm are presented in Figure 26 and Figure 27. The average shear stresses along the plates with different lengths for both cases are listed in Table 5 and Table 6. In Figure 26, it can be observed that the stresses in the middle part of the plates are smoother and there are stress concentrations in the areas close to the ends of the plates. It is interesting to see that for plates with different lengths, the pattern of the stress concentration at the top and bottom ends of the three plates are similar. In Figure 27, it is shown that the stress concentrations at the two ends of the plates can be ignored. Specifically, for the 50 mm and 75 mm long plates, the stresses along the plates are close to a constant value, which can also be verified in Table 6. For the longest plate with a length of 100 mm, there is a stress drop close to the top of the plate. Since the distance of the top of the plate to the free surface is only 30 mm, it may cause a stress deficiency at the location close to the top of the plate. Actually, this phenomenon can also be observed for case I in Figure 26.

It was concluded that for Bingham type fluids such as bentonite suspension B3, plates with shorter length can be used and the end effects can be neglected. For Hershel-Bulkley type fluids such as bentonite suspension B1, a correction factor has to be computed in order to obtain accurate yield stress values. This would imply that to determine whether the end effects are significant, the type of rheological material (Bingham or Hershel-Buckley) needs to be known a priori. If the type of rheological material is not known, then it should be assumed that the end effects need to be considered.

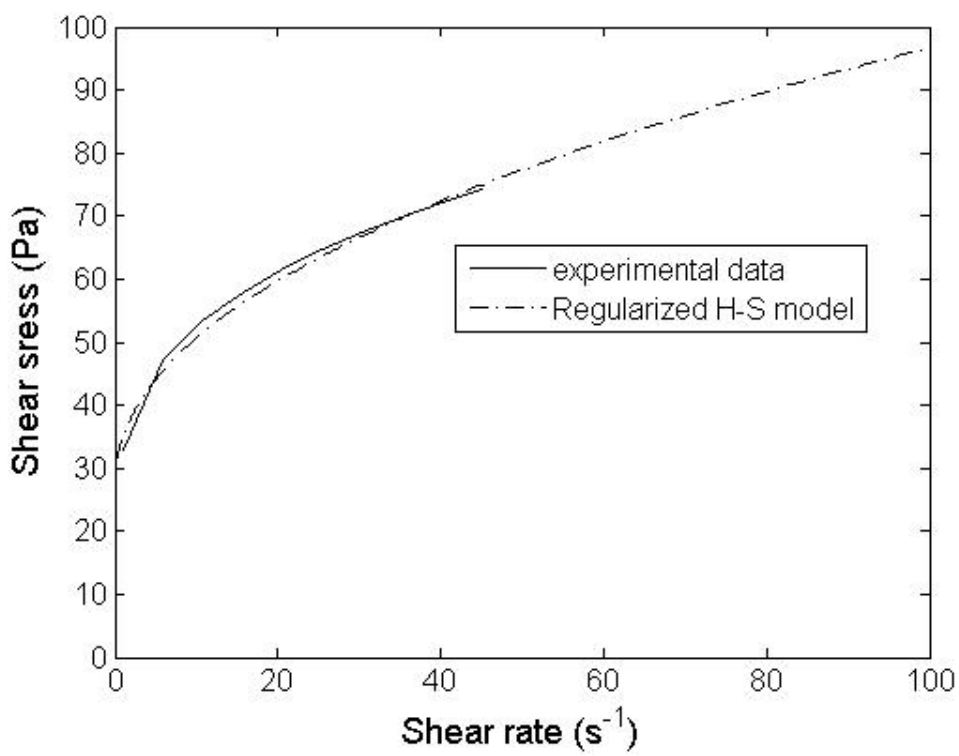

Figure 20: Comparison of shear stress versus shear rate for Case I (bentonite suspension B1). The experimental data were obtained using conventional rheometers (see section 4.2)

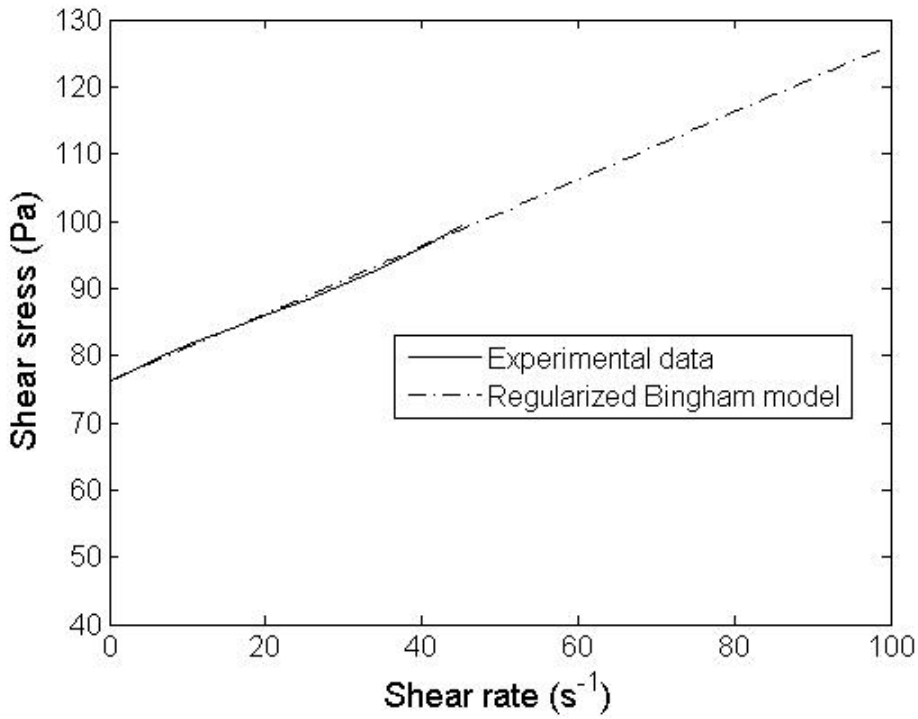

Figure 21: Comparison of shear stress versus shear rate for Case II (bentonite suspension B3). The experimental data were obtained using conventional rheometers (see section 4.2)

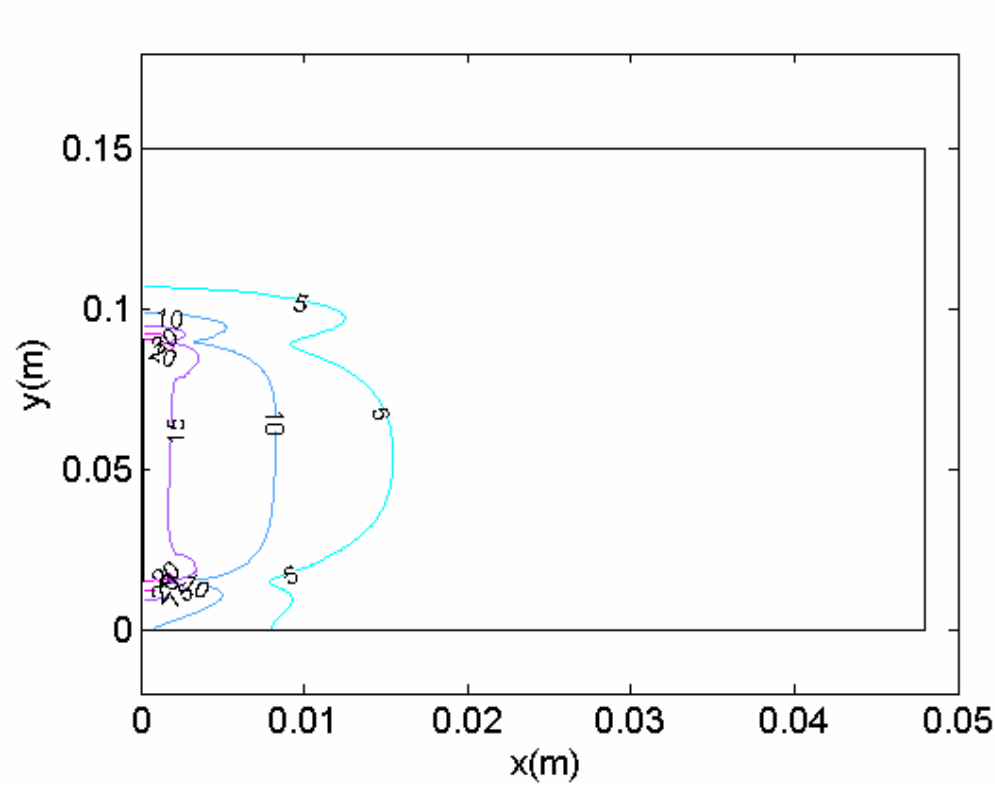

Figure 22: Contour plot of shear stress (Pa) for bentonite suspension B1 (case I).

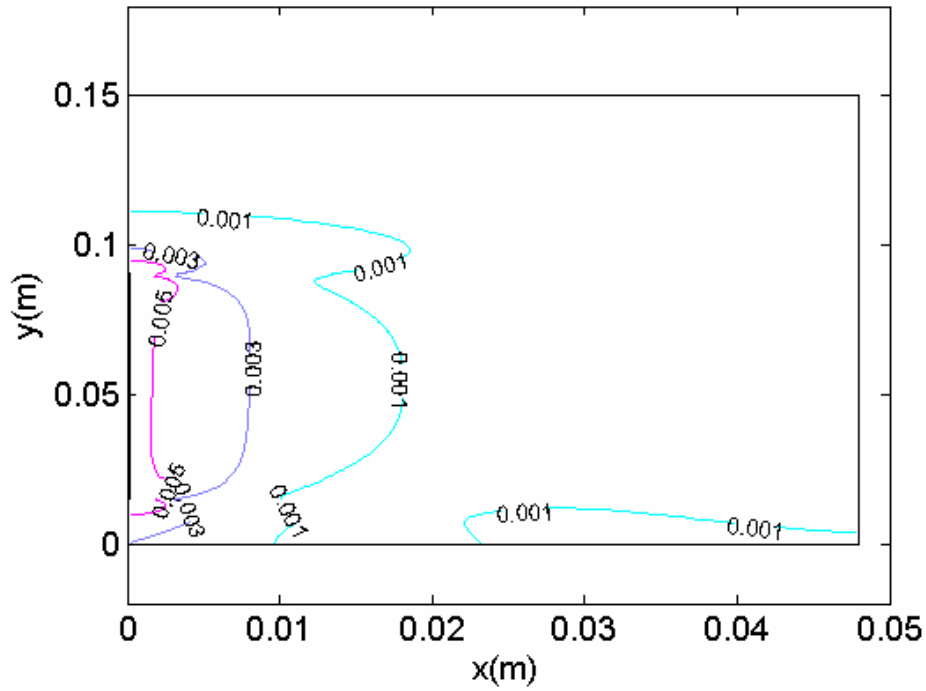

Figure 23: Contour plot of shear rate (1/s) for bentonite suspension B1 (case I).

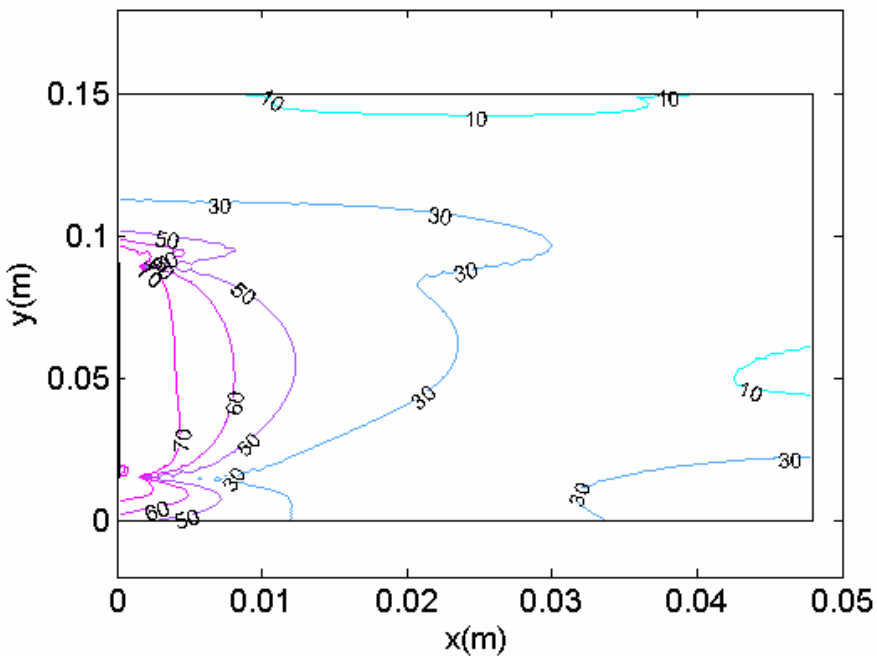

Figure 24: Contour plot of shear stress (Pa) for bentonite suspension B3 (case II).

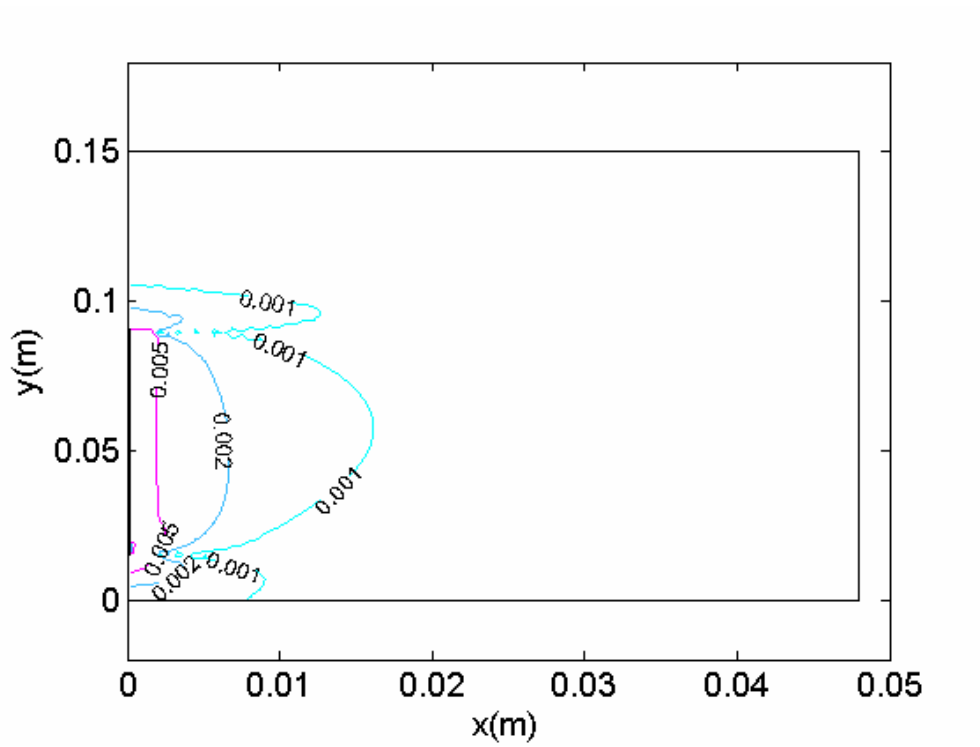

Figure 25: Contour plot of shear rate (1/s) for bentonite suspension B3 (case II).

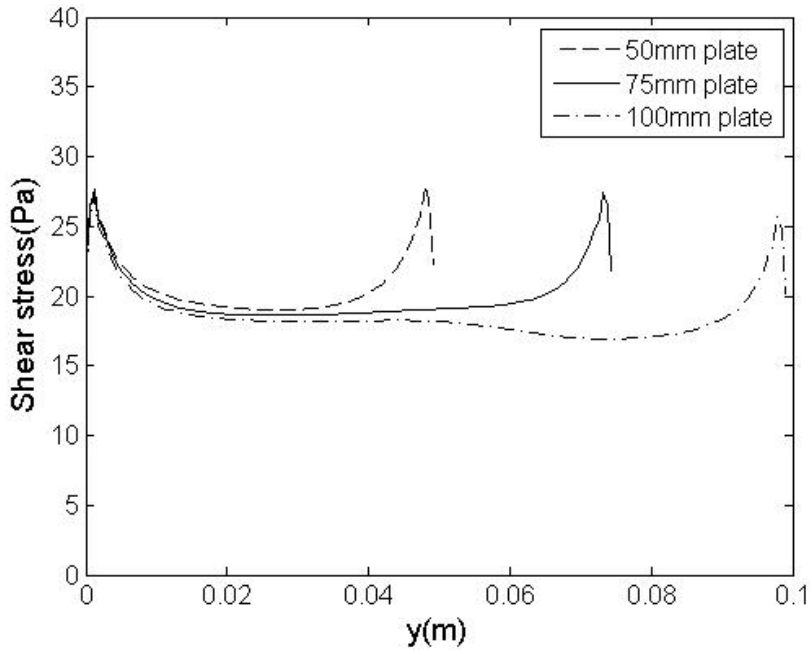

Figure 26: Stress distribution along plates of different lengths for case I (bentonite suspension B1). The top of the plate is at y =100 mm and the bottom of the plate is at y = 0. mm

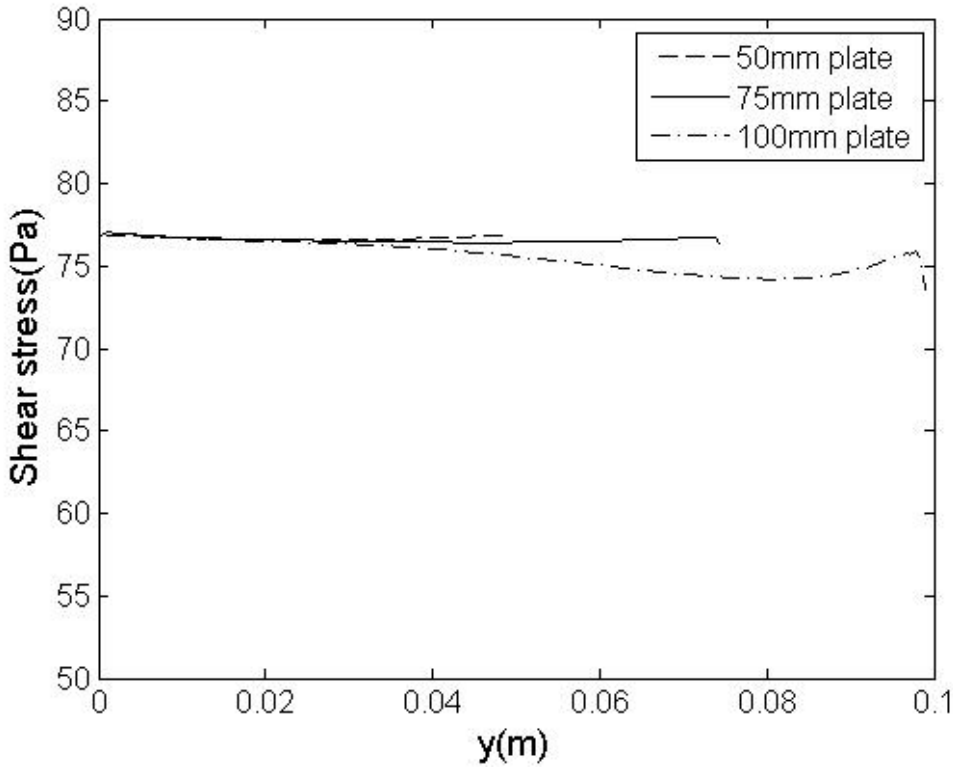

Figure 27: Stress distribution along plates of different length for case II (bentonite suspension B3). The top of the plate is at y =100 and the bottom of the plate is at y = 0.mm

Table 5: **Average shear stress along the plates of different length for Case I (bentonite suspension B1)**

Plate length	50 mm (SP)	75 mm (MP)	100 mm (LP)
Shear stress (Pa)	20.8	19.9	18.6

Table 6: Average shear stress along the plates of different length for Case II (bentonite suspension B3)

Plate length	50 mm (SP)	75 mm (MP)	100 mm (LP)
Shear stress (Pa)	76.7	76.6	75.6

6. Results and Discussion

6.1. Determination of yield stress from the slotted plate device

6.1.1. Interpretation of the measurements

Yield stress may be calculated based on the net force at Point *A* or Point *B* shown in Figure 6 (section 2). Some researchers [21, 22, 23] suggest that the shear stress calculated from the force at Point *B* corresponds to complete break down of the fluid structure and hence is a measure of the yield stress. However, other studies [24, 25, 26] suggest that the non-linear region from Point *A* to *B* is a function of the applied shear rate and that yield actually starts at Point *A* where the curve deviates from linearity. The yield stress corresponding to the shear stress at Point *A* is often referred to as static yield stress (τ_{st}) since macroscopic flow has not occurred. The stress at the peak of the shear stress-time curve is often referred to as dynamic yield stress (τ_d), denoting the onset of viscous flow. According to Nguyen & Boger [6], these two yield stresses might be lower and upper yield stress values corresponding to the end of the elastic deformation and start of fully viscous flow, respectively.

Figure 28 compares typical curves of the force response with time determined from the plate device using the MPS (75 mm/no slot and sand blasted) plate (column (a)) and typical curves of the shear stress vs. shear rate determined from the co-axial rotational rheometer for the suspensions tested (column (b)).

Practically, it is easier to determine the maximum value than the point where the force response - time curve departs from linearity, particularly for the cement paste and TiO_2 suspension. For these two suspensions, the force - time curves were not smooth as those of the bentonite suspensions, which make the determination of the points where the force – time curves depart from linearity more difficult. Thus, the yield stress calculated from the force at the Point *B* (maximum) would have less error than that calculated from the Point *A*, and was therefore used in this work. The decision to use Point B instead the Point A (representing the yield stress independent from shear rate) is acceptable here because the comparison is between results obtained using the same shear rate. This result can also be compared with the rotational rheometer since the yield stress is recorded at the onset of the viscous flow.

From Figure 28, it appears that the flow (measured using the rotational rheometer) of the bentonite suspensions B2 and B3 may be approximated by the Bingham model, whereas that of the cement paste, bentonite B1, and TiO_2 suspensions may be approximated by the Hershel-Buckley model. It is not clear if B2 and B3 behave similarly because their composition is similar while B1 had a different composition (see 4.1.2.).

The uncertainty of the results is estimated to be about 10 % for the measurements with the rotational rheometer [14, 27]. For the tests using the plate device, the estimation of the uncertainty was harder due to the limited number of tests performed with this device.

	Typical force response with time determined from the plate device using the MPS plate	**Typical curve of shear stress vs. shear rate determined from the co-axial rotational rheometer**
Cement paste M	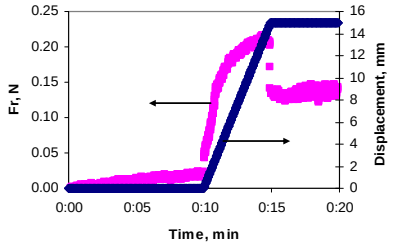	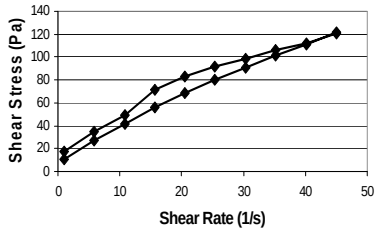
Bentonite suspension B1	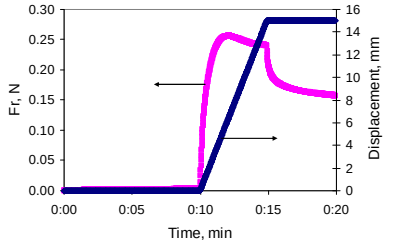	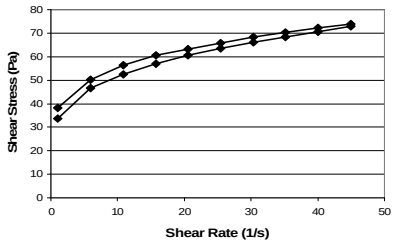
Bentonite suspension B2	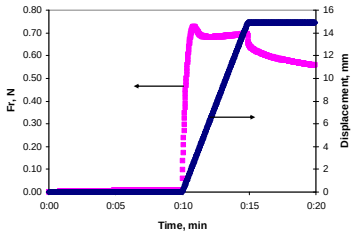	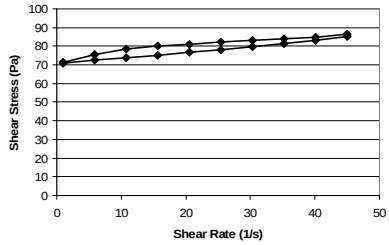
Bentonite suspension B3	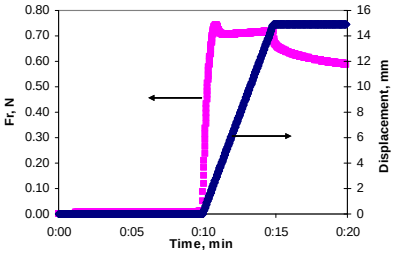	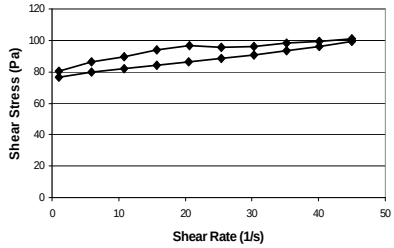
TiO_2 suspension (A parallel plate was used instead of co-axial rotational rheometer)	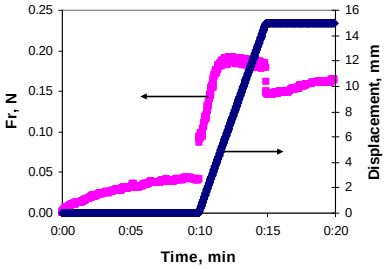	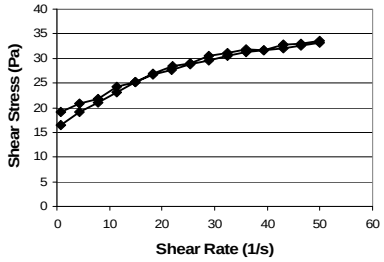
	(a)	(b)

Figure 28: Comparison of typical curves of the force response with time determined from the plate device using the MPS plate (a) and those of the shear stress vs. shear rate determined from the co-axial cylinder rheometer (b). The data are from on measurements but the uncertainty is estimated to be 10 %.

6.1.2. Edge effect correction

According to the numerical simulation presented in the previous section (section 5), it was concluded that:

- for the Bingham type fluids, shorter length plates can be used and the end effect can be ignored, and
- for the Hershel-Bulkley type fluids, a correction factor has to be computed in order to obtain accurate yield stress values.

The mean shear stress for the slotted and non-slotted plates was calculated with and without the consideration of an edge-effect correction, and the comparisons are presented in Table 7 and Table 8 for the sand blasted and non-sand blasted plates, respectively.

From Figure 28, it would appear that cement paste and bentonite B2 and B3 have no end effects, while the bentonite B1 and TiO_2 should have a correction factor due to end effects. In Table 7 and in Table 8, the mean stress for all material is shown. Also the percentage differences between the values without edge correction and with edge corrections are calculated in relation of the values with edge effect correction. From the results shown in the tables (Table 7, Table 8), it seems that for the B2 and B3 bentonite suspensions, consideration of the edge-effect correction in the calculation of the mean shear stress τ resulted in relatively small differences of less than 16 % compared with that without the edge-effect correction, as predicted by the numerical simulation. For the bentonite B1, the differences were over 20 %, considered significant, in agreement with the numerical simulation. For the TiO_2 suspension, the difference was relatively small (9 %) when sand blasted plate was used (Table 7), but significant (about 80 %) when smooth plate was used (Table 8). Thus no clear trend was observed. For the cement paste, however, the difference on the shear stress calculated with or without the consideration of the edge correction was substantial, in contradiction with the numerical simulation. The authors have no explanation at this time for the reason of the discrepancy.

For further comparison, therefore, the shear stress with the consideration of edge correction was used. Discussion of these results is presented in section 6.1.3.

Table 7: Mean shear stress τ comparison (sand blasted plates). The uncertainty is estimated at 10 %.

	With edge effect correction		Without edge effect correction		% difference in τ with or without edge correction	
	τ [Pa]	τ [Pa]	τ [Pa]	τ [Pa]		
Plate type	MPS	SL11	MPS	SL11	MPS	SL11
	$\beta = 0$	$\beta = 0.358$	$\beta = 0$	$\beta = 0.358$	$\beta = 0$	$\beta = 0.358$
Cement paste	14.6	30.6	29.2	45.1	100	47
Bentonite B1	25.7	24.2	32.0	30.5	25	26
Bentonite B2	80.5	74.0	88.9	82.3	10	11
Bentonite B3	84.8	80.0	97.2	92.4	15	16
TiO_2 suspension	21.5	21.0	23.4	22.9	9	9

Table 8: Mean shear stress τ comparison (smooth, non-sand blasted plates) The uncertainty is estimated at 10 %.

	With edge-effect correction		Without edge-effect correction		% difference on τ with or without edge correction	
	τ [Pa]	τ [Pa]	τ [Pa]	τ [Pa]		
Plate type	MP	SL14	MP	SL14	MP	SL14
	β = 0	β = 0.455	β = 0	β = 0.455	β = 0	β = 0.455
Cement paste	5.8	23.8	26.7	44.7	360	88
Bentonite B1	26.3	25.1	31.5	30.2	20	20
Bentonite B2	71.5	73.1	81.4	83.0	14	14
Bentonite B3	70.5	77.9	81.8	89.2	16	15
TiO_2 suspension	11.4	11.5	20.6	20.7	81	80

6.1.3. Comparison of yield stress from the slotted and non-slotted plates

Table 7 and Table 8 show that for the bentonite and TiO_2 suspensions, the mean shear stress τ determined from the slotted and solid plates was not significantly different. It was also observed in the experiments that for these suspensions, when the plates (both sand-blasted and smooth) were pulled from the suspensions, the maximum shear strain was probably not through the boundary between the plate surfaces and the suspensions; thin layers of the suspensions were adhering to the plates (so there was almost no slippage). This non-slippage of bentonite on steel surfaces was also observed by Mannheimer [28]. Figure 29 shows an example for bentonite suspension B1. This indicates that the shear was not through the boundary between the plate surface and the suspension, but through the bentonite suspension in a thin layer away from the plate. The calculation of yields stress using the plate device relies on equation (3) that considers that τ_S and τ_B as two independent entities. If there is no slippage and τ_S and τ_B are identical, the yield stress cannot be calculated using equation (3) [3]. The results obtained for these suspensions are not consistent with those reported by Zhu et al [3]. They reported (see section 2) that the yield stress increases with β as shown in Figure 3 and with no slippage the stress measured is independent of β.

For the cement paste, the shear stress from the solid (non-slotted) plate was lower than that for the slotted plate, and the slippage appears to be between the plate and the cement paste. This is consistent with the results of Zhu et al. [3].

Because of the above observed differences between suspensions, the yield stress of the cement paste and the other suspensions was calculated via different approaches. For the cement paste, the yield stress τ_B was calculated according Equation (4). For the other suspensions, the yield stress was considered as the mean yield stress exerted over the plate surface, ie. $\tau_B = \tau$ was calculated according to Equation (1) [$\tau = (F_r - F_e)/2\ WL$] using the test results from the MPS and MP plates since the shear forces were through the suspensions.

Figure 29: Picture showing the bentonite suspension B1 on the smooth medium plate SL11 when the plate was pulled out of the suspension

6.2. Comparison of yield stress of the materials determined by different rheometers and methods

The yield stress of the suspensions determined by different rheometers and procedures are summarized in Table 9

Yield stress measurements are affected by the time scales of the experiment [6]. The longer the measurement times (the lower the shear rate), the smaller the yield stress value. A stress growth mode was used for the tests with the parallel-plate rheometer and the plate device. Comparing the results from these two tests, the yield stress is reached in a few seconds while using a parallel plate test, and in approximately 100 s in a plate test. The values obtained for the cement paste and bentonite and TiO_2 suspensions are thus lower with the plate tests than those by the parallel-plate rheometer. Another factor that might have contributed to differences between the yield stress determined by the parallel plate rheometer and by plate device was the surface texture of the plates. For the parallel-plate rheometer, serrated plates were used for the tests except for the TiO_2 suspension. Sand blasted and smooth plates were used with the plate device.

Comparing the results from the test by the co-axial rotational rheometer and the parallel-plate rheometer (Table 9) it is seen that the parallel plate results are almost always higher than those of the co-axial cylinder rheometer. One exception is the bentonite B1 suspension. These discrepancies can be explained by the difference in the type of measurements. The yield stress by parallel plate was determined by a stress growth method, implying that the structure of the material was not disturbed prior to the test. On the other hand, the co-axial cylinder measurements were performed using a Bingham model. The Bingham yield stress involves an extrapolation to zero shear rate while the measurements are done from 50 s^{-1} to 0.5 s^{-1}. The structure of the material is destroyed during the high shear portion of the test and therefore the yield stress obtained will be lower. Another factor that might have contributed to the difference for the yield stress

determined via the parallel-plate and coaxial cylinder rheometers was the surface texture of the plates and cylinder rotor. Parallel plates had serrated surfaces, whereas the cylinder rotor and inner wall of outer cylinder were smooth.

As mentioned earlier, the MPS and SL11 plates were sand blasted, whereas the MP and SL14 plates were smooth and without surface treatment. Table 9 shows that the yield stress of the suspensions determined by the sand blasted plates was higher than that determined by the smooth surface plates except for bentonite suspension B1, which showed similar values yield stress between the two kind of plate surfaces. This suggests that the surface texture of the plates does affect the yield stress measurement of the suspensions as in other types of rheometers. This finding seems to be consistent with that reported by Zhu et al. [3].

Table 9: Comparison of yield stresses determined by the slotted plate device and other rheometers. The uncertainty is estimated at 10 %.

	Yield stress, Pa			
	Rheometer		Plate device	
	parallel-plate configuration (stress growth, shear rate 0.1 s^{-1})	co-axial cylinder configuration (Bingham, shear rate 50 – 0.5 s^{-1})	sand blasted plates (stress growth, shear rate 0.005 – 0.006 s^{-1})	smooth plates (stress growth, shear rate 0.005 – 0.006 s^{-1})
Cement paste	108	13.2	59.2	45.3
Bentonite suspension B1	40.9	40.8	25.7	26.3
Bentonite suspension B2	93.2	70.2	80.5	71.5
Bentonite suspension B3	119.0	77.5	84.8	70.5
TiO_2 suspension	26.7*	21.6**	21.5	11.4

* Tests were done using a pair of disposable parallel plates without serration due to the difficulty in cleaning the serrated plates.
** Tests were done using a pair of disposable parallel plates instead of co-axial cylinders.

6.3. Other observations from the tests using the plate device

6.3.1. Force measured without plate movement

Figure 28a shows that for the cement paste and the TiO_2 suspensions, the net force F_r increased with time in the first 10 min before the plate started to move in the suspensions. This phenomenon was not observed for the bentonite suspensions. Although it is not clear why this increase is occurring, several hypotheses could be advanced.

The difference between bentonite and cement paste/ TiO_2 behavior might be attributed to several factors, such as volume concentration of the suspension, physical properties of the particles in the suspension, and/or the degree of particle flocculation (inter-particle distance). Unfortunately, the data available cannot allow us to determine which of the above factors would be the most significant. Table 10 shows the yield stress and plastic viscosity of the suspensions determined by the co-axial rotational rheometer in relation to the volume concentration of the suspensions. The bentonite suspensions had much lower volume concentration than the cement paste and the TiO_2 suspension. For a given type of suspension, the increase in the solid volume generally leads to an increase in the viscosity of the suspension (TiO_2 was measured with a smooth surface and could have lead to a lower or viscosity then expected).

Table 10: Yield stress and plastic viscosity of the suspensions determined by the co-axial rotational rheometer. The uncertainty is estimated at 10 %.

	Volume concentration, %	Yield stress, Pa	Plastic viscosity, Pa s
Cement paste	48	13.2	2.4
Bentonite suspension B1	3.9	40.8	0.8
Bentonite suspension B2	3.1	70.2	0.3
Bentonite suspension B3	3.1	77.5	0.5
TiO_2 suspension	20	21.6*	0.2*

* Tests were done using a pair of disposable parallel plates.

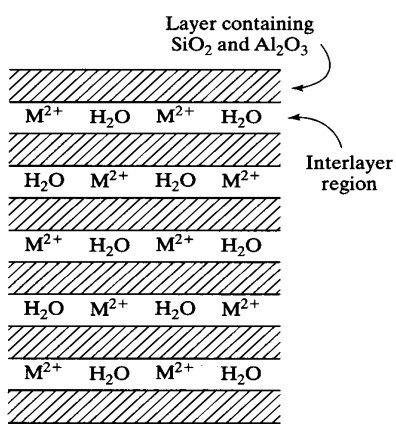

Figure 30: Schematic model of well crystallized clay mineral [26]

The bentonites are impure clays consisting mostly of montmorillonites. Most clay minerals consist of layers that are stacked parallel to each other (Figure 30). In the suspensions the bentonite particles absorb water, possibly several times their original dry mass [25], between the layers containing SiO_2 and Al_2O_3. This results in expansion and swelling of the particles, increase in the volume concentration, and reduction in the inter-particle distance. The suspensions may behave as gels or "concentrated" suspensions so that there is either no settling of the swollen bentonite particles in the gels or unnoticeable over the 10 min experimental procedure and limited settling of the particles in the

concentrated suspensions. The cement paste had limited hydration at short times, particularly when the retarder admixture was added (Figure 10); the paste behaves as a suspension. Due to the difference of specific gravity between cement and water, the cement particles might have settled in the first 10 min even before the plate moved through the paste. This may be the reason of the increase in the net force F_r with time registered in the first 10 min. This may also be the case for the same phenomenon observed with the TiO_2 suspension. An increased sedimentation implies a downward movement of the particles against the plate. In this movement the plate is pulled down and thus an increase of the force F_r is measured.

A further observation for materials with a stress increase during the first 10 min is that there is also an increase during the relaxation period (following point C in Figure 6). A possible explanation is that a small vertical deformation could generate a shear stress at the plate surface, leading to a mass increase in the balance. This can be due to a vertical consolidation and/or a vertical deformation under the material's own weight. In cement paste, the origin of this deformation was explained by Ovarlez and Roussel [29] by the small settling that can always be measured at the surface of any freshly cast concrete. If cement paste at rest (below the yield stress) behaves as an elastic solid, a deformation (shear strain) must be at the origin of the shear stress that is exerted on the plate by the cement paste. The shear strain for cement paste that would induce the paste to yield (critical strain) is relatively low, about 0.0005 [30]. Even a small deformation could generate a large part of the yield stress, since until the critical strain, the stress increases linearly due to the elastic behavior of the material at rest. Tchamba et al. [31] observed that the shear stress at the surface of a static plate increases with time, (i.e. the balance records an increase in mass with time). This shear stress could reach, in specific cases, the yield stress value using a static plate simply immersed into cement paste, without any motion.

In bentonite the situation is different as no increase of the stress is detected in the first 10 min (Figure 6). This could be due to the fact that bentonite has a critical strain of the order of 0.1 and therefore a higher deformation is needed to overcome the yield stress. As no increase is detected, this would imply that the particles are not moving significantly in the time frame of the experiment (10 min). Bentonite does not sediment as easily at the concentration used as cement paste leading to no strain and no therefore no stress on the plate at rest. In other words, the strain rate generated at the interface between the plate and the material is small and always lower than the critical strain rate. That is: the shear stress on the plate has an unknown value between zero and the yield stress and cannot be detected on the balance, thus the shape of the curve seen in Figure 6.

6.3.2. Experimental issues with concentrated suspensions

One of the difficulties in the test with the plate device for concentrated suspensions is to ensure that the plate is in a vertical position. This is particularly difficult in the case of cement pastes. If the plate is not in a vertical position, it will cause errors because the force measured would be higher than for a vertical place due to other factors than yield stress.

Another difficulty in determining the yield stress by the plate device resides with the experimental time. Since the shear stress τ_S is associated with the suspension to be tested, the determination of edge effect correction is essential for suspensions such as cement pastes. This means that the correction factors have to be determined for cement pastes with different w/c ratios or with different types or dosages of admixtures. In order to determine this correction factor, time consuming tests using small, medium, and large plates are required. Cement experiences hydration when in contact with water and the yield stress of the cement pastes increases with time after an initial dormant period. This makes the accurate yield stress determination difficult. In this report a retarder was added to allow the cement paste to be stable for 4 h but the test should be designed for a wide range cement paste composition and not only the cement paste with a retarder.

7. Summary and Conclusions

The determination of the true yield stress is essential in the description of the flow of suspensions such as cement pastes. A simple rheometer was designed for measuring the yield stress in concentrated suspensions. The scope of this study was to assess whether this newly developed slotted plate device [3, 4] would be usable for dense suspensions such as cement pastes.

A device similar to the one used by Zhu et al. [3, 4] was built at NIST. The device was modified to accommodate highly concentrated suspensions with larger particles than used by Zhu et al.[3]. Bentonite, cement paste, and TiO_2 suspensions were measured.

Careful tests were conducted using various plates as outlined by Zhu et al. [3] and analyses of the results were conducted both analytically and via computer simulations. Traditional rotational rheometers were used for comparison as well as to provide data for the computer simulations.

The simulations of the plate device show that the end effects (drag force on the upper and lower edges of a plate moving in the suspension) depended on the type of material being measured. For instance, a Hershel-Buckley material shows a large stress increase at the edge of the plates, while a Bingham material had a negligible stress. This would make the interpretation of the experimental results harder as the type of correction needed might not be known a priori.

The results obtained were not as clear as was first expected. The interpretation is not conclusive and further developments are needed, both in experimental work and in simulation, to adopt this method for concentrated suspensions such as cement pastes.

8. References

1 Hackley, V. A. and Ferraris, C. F., (2001) "The use of nomenclature in dispersion science and technology," NIST Recommended Practice Guide, SP-960-3.

2 ACI 238-1R- 07, (2007) "Report on Measurements of Workability and Rheology of Fresh Concrete"

3 Zhu L, Sun, N, Papadopoulos, K, and De Kee, D., (2001) "A slotted plate device for measurement static yield stress," J. Rheology, 45 (5), pp. 1105-1122.

4 Zhu H, De Kee D., (2006) "Slotted-plate Device to Measure Yield Behavior of Powders; FEM Analysis", Ind. Eng. Chem. Res., vol.45, pp. 5375-5383.

5 Banes, H. A. and Walters, K., (1985) "The yield stress myth?," Rheol. Acta, 24, pp. 323-326

6 Nguyen Q. D. and Boger D. V.,(1992) "Measuring the Flow Properties of Yield Stress Fluids", Ann. Rev. Fluid Mech., **24**, pp. 47-88.

7 Zhu, L., Papadopoulos, K. and De Kee, D., (2002) "Yield Stress Measurement of Silicon Nitride Suspensions", Can. J. Chem. Eng., **80** pp. 1175-1180.

8 Picandet, V., Ferraris C., De Kee D., (2007) "Novel rheometer to measure yield stress of suspensions", 5th International RILEM Symposium on Self-Compacting Concrete, Ghent, Belgium, pp 335-340.

9 Zhu, L., Papadopoulos, K. and De Kee, D., (2002) "Yield Stress Measurement of Silicon Nitride Suspensions", Can. J. Chem. Eng., **80** pp. 1175-1180.

10 Amziane S., Ferraris C.F. (2007) "Cementitious Paste Setting Using Rheological and Pressure Measurements", ACI Materials Journal, vol. 104 #2, pp. 137-145

11 Lombardi G., (1985) "The role of Cohesion in Cement Grouting of Rock", Proc. of 15th Intern. Congress on Large Dam, Lausanne (Switzerland), pp. 235-261

12 Carroll D.,(1970) "Clay Minerals: A Guide to Their X-Ray Identification", The Geological Society of America Special Paper 126, 80 pp.

13 Nguyen, Q. D., Akroyd, T., De Kee, D., and Zhu, L., (2006) "Yield stress measurement in suspensions: an inter-laboratory study," Korea-Australia Rheology Journal, 80 (1), pp. 15-24.

14 Ferraris, C. F., Obla, K., and Hill, R., (2001) "The influence of mineral admixtures on the rheology of cement paste and concrete," Cement and Concrete Research, 31 (2), pp. 245-255.

15 Lucy, L. B., (1977) "A numerical approach to the testing of the fission hypothesis", Astron. J. 83, pp. 1013- 1024.

16 Gingold, R. A. and Monaghan, J. J. "Smoothed particle hydrodynamics theory and application to non-spherical stars", Mon. Not. R. Astron. Soc. 181, pp.375-389 (1977).

17 Papanastasiou, T. C., (1987) “Flows of Materials with Yield”. J, Rheol. 31 , pp. 385-404 .

18 Alexandrou, A. N. , P. Le Menn, G. Georgiou, V. Entov, (2003) “Flow instabilities of Herschel–Bulkley fluids”, J. Non-Newtonian Fluid Mech. 116 pp. 19-32.

19 Burgos, G. R. and A. N. Alexandrou, V. Entov, (1999) ,”On the determination of yield surfaces in Herschel–Bulkley fluids”, J. Rheol. 43 pp. 463-483.

20 Zhu, H. and D. De Kee, (2007) “A numeric study for the cessation of Couette flow of non-Newtonian fluids with a yield stress”, J. Non-Newtonian Fluid Mech. 143 pp. 64-70.

21 Pryce-Jones, J., (1952) “Studies in thixotropy,” Kolloid-Z, 129, pp. 96-122.

22 Van den Tempel, M., (1971) “Structure of multiphase systems,” in Elasticity, plasticity and structure of matter, ed. R. Houwink, H. K. de Decker, pp. 123-137, Cambridge, Cambridge Univ. Press.

23 Papenhuijzen, J.M.P., (1972) “The role of particle interactions in the rheology of dispersed systems, Rheol. Acta, 11, pp. 73-88.

24 Mewis, J. and Meire, C., (1984) “Yielding in weakly flocculated systems,” in Advances in rheology, ed. B. Mena, A.Garcia-Rejon. C. Rangel-Nagaile, 2: pp. 591-598, Mexico City, Univ Nac. Auton. Mex.

25 Lin S.-F. and Brodkey, R. S., (1985) “Rheological properties of slurry fuels,” Rheol. 29, pp.147-175.

26 Nagase, Y. and Okada, K., (1986) “Heterogeneous behavior after yielding of solid suspensions,” J. Rheol, 30, pp. 1123-1142.

27 Ferraris C. F.,(2006) “Concrete Rheology: Knowledge and Challenges” 2nd International RILEM Symposium on Advances in Concrete Through Science and Engineering, Quebec, Canada (CD)

25 Luckham, P. F. and Rossi, S, (1999) “The colloidal and rheological properties of bentonite suspensions,” Advances in Colloid and Interface Science, 82, pp. 43-92.

26 Mindess, S., Young, J. F., and Darwin, D., (2003) *Concrete*, 2nd edition, Prentice Hall.

28 Mannheimer R. J., (1990) “Laminar and Turbulent Flow of Cement Slurries in Large Diameter Pipe – A Comparison with Laboratory Viscometers”, Proc. Int. Conf. British Soc. of Rheology “Rheology of Fresh Cement and Concrete” , Liverpool UK, pp. 147-158

29 Ovarlez G. and Roussel N., (2006), A Physical Model for the Prediction of Lateral Stress Exerted by Self-Compacting Concrete on Formwork, Materials and Structures, Volume **39(2)** pp. 239-248.

30 Struble, L.J., Schultz, M.A., (1993), Using creep and recovery to study flow behaviour of fresh cement paste, Cement and Concrete Research **23** pp. 1360-1379.

31 Tchamba J.C., Amziane S., Ovarlez G., Roussel N., (2007) “Lateral stress exerted by fresh fluid concrete on formwork: laboratory experiments”, Cement and Concrete Research, in press.